uOttawa

L'Université canadienne
Canada's university

FACULTÉ DES ÉTUDES SUPÉRIEURES ET POSTOCTORALES

uOttawa

L'Université canadienne
Canada's university

FACULTY OF GRADUATE AND POSDOCTORAL STUDIES

Steven Craig MAGUIRE

AUTEUR DE LA THÈSE / AUTHOR OF THESIS

M.Sc. (Chemistry)

GRADE / DEGREE

Department of Chemistry

FACULTÉ, ÉCOLE, DÉPARTEMENT / FACULTY, SCHOOL, DEPARTMENT

Magnetic Field Control of Silver Nanoparticle Formation

TITRE DE LA THÈSE / TITLE OF THESIS

Dr. T. Scaiano

DIRECTEUR (DIRECTRICE) DE LA THÈSE / THESIS SUPERVISOR

CO-DIRECTEUR (CO-DIRECTRICE) DE LA THÈSE / THESIS CO-SUPERVISOR

EXAMINATEURS (EXAMINATRICES) DE LA THÈSE / THESIS EXAMINERS

Dr. S. Barry

Dr. M. Murugesu

Dr. A. Sayari

Gary W. Slater

Le Doyen de la Faculté des études supérieures et postdoctorales / Dean of the Faculty of Graduate and Postdoctoral Studies

Magnetic Field Control of Silver Nanoparticle Formation

Steven Maguire

A thesis presented to the

Faculty of Graduate and Postdoctoral Studies

In partial fulfillment of the requirements for the degree of

Master of Science

In the Ottawa-Carleton Chemistry Institute

Department of Chemistry, University of Ottawa

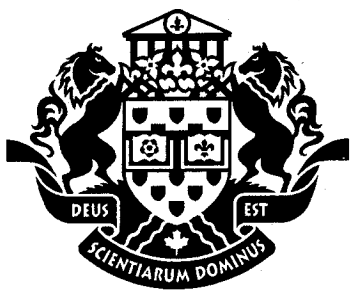

Université d'Ottawa • University of Ottawa

Candidate

Steven Maguire

Supervisor

Professor J. C. Scaiano

Your file Votre référence
ISBN: 978-0-494-25803-3
Our file Notre référence
ISBN: 978-0-494-25803-3

Abstract

Silver nanoparticles can be readily generated in micellar environments by ketyl radicals formed from the photoreduction of benzophenone in the presence of a suitable hydrogen donor. The yield of these ketyl radicals can be increased by extending the lifetime of the triplet radical pair through Zeeman splitting of the triplet sublevels in an externally applied magnetic field. This provides control over the rate of photogeneration of nanoparticles under very mild conditions. The rate of photogeneration can be monitored by the distinctive surface plasmon resonance absorption around 420 nm. In this work, micelles of sodium dodecyl sulphate (SDS) were employed, and 1,4-cyclohexadiene (1,4-CHD), an excellent hydrogen donor, was used to promote the generation of ketyl radicals. When benzophenone and a silver salt are added to this system and it is irradiated in the presence of a magnetic field, the rate of appearance of the plasmon band is enhanced. In addition to serving as a hydrogen donor, 1,4-CHD also has a stabilising influence on the nanoparticles, adsorbing onto the surface and preventing aggregation. 1,4-CHD added to a solution of nanoparticles synthesised without the diene present will even break up existing aggregates.

Acknowledgements

I would like to thank Dr. J.C. (Tito) Scaiano, my supervisor, for showing just the right amount of patience with me and for giving me a chance to go to grad school. I would also like to thank Dr. Carolina Aliaga for a judicious prod when necessary.

My parents, Ron and Alison Maguire, provided sage advice in the bleakest days of dark despair, and also plane tickets home for Christmas.

My labmates, specifically Dr. Michelle Chretien, Dr. Matthew Lukeman, Dr. Carlos Sanrame, Dr. Belinda Heyne, Dr. Claudio Carra, Mathieu Frenette and Kathy-Sarah Focsaneanu were always available to answer my questions. In addition, Mark Perry, Jessie Blake, Kathy McGilvray, Larisa Mikelsons, Marius Ivan, Marie Laferrière, Dr. Vincent Maurel, Dr. Raquel Galian, Vasilisa Filippenko, Rob Goudin and Matt Decan were always available to help me procrastinate. I would like to specifically thank Gino Cuglietta for help with the lasers, Betty Yakimenko for a thousand and one administrivial details looked after, and Dr. Colleen Sutton for going above and beyond the call of duty proof-reading this thesis.

I would also like to thank Dashan Wang of the National Research Council of Canada's Institute for Chemical Process and Environmental Technology for graciously providing TEM time and technical support.

Finally, I would like to thank Dr. Keith Ingold for talking me into going waterskiing when I should have been working.

Table of Contents

Table of Contents

List of Figures

Chapter 1

List of Schemes

Chapter 1

List of Tables

Chapter 1

Table of Equations

Abs	absorbance
ACN	acetonitrile
BP	benzophenone
BPK	benzophenone ketyl radical
1,3-CHD	1,3-cyclohexadiene
1,4-CHD	1,4-cyclohexadiene
CTAN	cetyltrimethylammonium nitrate
ΔAbs	change in absorbance
ΔO.D.	change in optical density
FTIR	Fourier-Transform Infrared spectroscopy
fwhm	full-width half maximum
k_{obs}	observed rate constant
kV	kilovolt
LFP	Laser Flash Photolysis
λ_{max}	peak absorbance wavelength
M	moles per litre (Molar)
MeOH	methanol
MM	milliMolar
Ms	millisecond
MT	milliTesla
nm	nanometre
ns	nanosecond
s	second
SDS	sodium dodecyl sulphate
SERS	Surface-Enhanced Raman Spectroscopy
TEM	Transmission Electron Microscopy
UV	ultraviolet

1.1. Introduction

1.1.1. Nanoparticle Background

Nanotechnology is a currently a burgeoning field in Canada and around the world, both in pure research and in product development. The National Institute for Nanotechnology in Edmonton, Alberta was recently established to bridge the gap between these two fields.[1] The word nanoparticle was first used in the chemical literature in 1976,[2] and for the last decade and a half the number of papers published involving nanoparticles has increased every year. Even before the term nanoparticle was coined, the concept of extremely finely divided particles suspended in solution was known or suspected as early as the 17th century.[3] Although there is currently no official definition of a nanomaterial, a commonly accepted working definition is a material having at least one physical dimension measuring less than 100 nanometres.[4] A material with only one dimension meeting this criterion is a nanofilm, and a material with two dimensions less than 100 nm is a nanorod or nanowire. A nanoparticle is a particle having all three dimensions measuring less than 100 nm.

In addition to spherical,[5] tetrahedral,[6] pentagonal,[7] octahedral[8] and other morphologies, nanoparticles are also known to occur in such exotic shapes as stars,[9] cups.[10] coils[11] and flakes.[12]

Nanotechnology offers the potential for new materials and new nanodevices as well. A recently published paper describes a "nanocar" with fullerene wheels and an alkyne-based suspension,[13] This car is capable of traversing a gold surface, rolling on its wheels when heated above 473K. A slightly different design of nanocar incorporates a molecular motor based on a helicene acting as a "paddlewheel" to lift and haul the car along the gold surface,[14] This motor is "fuelled" by photons, which induces rotation of the helicene.

When considering the size of nanoparticles and the surface-to-volume ratio, it can easily be seen that the number of atoms on the surface of the particle as a percentage of the total number of atoms making up the particle is much larger than the bulk material, where only a trivial fraction of atoms are on the surface. Because of this large surface area, interactions of the surface with the solvent allow the nanoparticles to be suspended in solution rather than precipitating out.[15]

Nanoparticles can be characterised by a number of instrumental techniques. Chief among them are scanning and transmission electron microscopy (SEM and TEM).[7] In the first case, SEM works by scanning an electron beam across the surface of a sample and assembling an image from the reflected electrons.[16] On the other hand, TEM instruments collect the electrons that are transmitted by the sample; darker regions of the image represent areas where the electron beam was either absorbed or reflected, indicated regions of greater material density.[16] Other useful techniques include powder X-ray diffractometry (XRD) for determining the crystal structure of the particles[17], Atomic

Force Microscopy (AFM, useful in imaging larger particles,[18] and X-ray photoelectron spectroscopy (XPS) for determining the surface properties of the material,[19] This last is a powerful technique not only because of the high surface-to-volume ratio already mentioned, but also because it reveals information about the surface capping ligands, which will be discussed later.

One of the major research aims of nanotechnology is the rational synthesis of nanoparticles – particles having three linear dimensions on the nanometer scale. Many unique and interesting properties not seen in bulk material arise at this scale.[20] The earliest systematically studied nanoparticles were made of organic polymers and used as drug delivery agents,[2] but in recent years particles of transition metals such as silver, gold and copper,[21-29] oxides of iron, nickel and cobalt[30-38] and semiconductors such as cadmium selenide or gallium arsenide[39-44] have been developed, finding use in applications as diverse as optical sensors,[45] electronics[46] and catalysts.[47-52] In addition, composite materials are also known, such as core-shell hybrids like zinc sulphide-capped cadmium selenide nanoparticles[53] or polymer-layered silicate nanocomposites.[54] Gold nanoparticles in particular have been used since the tenth century as a rose-coloured tint for stained-glass windows.[3] The antibacterial properties of silver nanoparticles have been harnessed in for applications to clothing by coating polymer fabrics with the nanoparticles.[55]

Techniques for the synthesis of nanoparticles include precipitation,[56-58] sol-gel condensation[59-61] and photogeneration.[62-69] The most common technique is to simply precipitate the particles from a supersaturated solution.[70] This can be accomplished by

the careful addition of concentrated reagents to a saturated solution, or by heating and cooling to achieve supersaturation. This causes a brief burst of nucleation followed by a slower particle growth. During this nucleation process, nuclei of a range of sizes are formed. These nuclei possess a minimal stable size called the critical radius, which is a function of the saturation ratio – the ratio of the concentration of the reactants to their theoretical solubility - of the solution. Nuclei smaller than the critical radius decompose and the smaller particles are incorporated into larger nuclei in a process called Ostwald ripening.[70, 71] A shorter nucleation period leads to fewer nuclei, which then experience less competition for material and hence grow larger. Particle size can therefore be tuned by controlling the length of time of this nucleation.

Precipitation is an ideal method of synthesis for nanoparticles of ionic materials such as cadmium selenide or indium arsenide, which can be prepared from salts of the respective ions, but metallic particles prepared from salts obviously require a reduction step. This can be accomplished by treating an ion-separated solution with a borohydride or other strong reducing agent.[72] Alternately, photochemistry can be employed to generate radical reducing species.[68] Photogeneration involves a continuous process of nucleation, rather than the brief burst characteristic of precipitation methods. As a result, the size distribution of the products depends more on the stability of the resultant particle than on the length of the nucleation burst. Photochemical-driven growth is also possible with nanoparticles that have been previously prepared according to precipitation or chemical reduction methods.[73] In addition, synthetic procedures are known whereby particles are photogenerated in polymer films.[67] These particles have the advantage of

being stabilized by the surrounding polymer, and can be synthesised *in situ* for applications requiring nanoparticle-loaded films, something inaccessible from precipitation methods.

Each nanoparticle species has a distinct absorption spectrum arising from the propagation of electromagnetic waves along the metal surface caused by the oscillation of electron density in the conduction band, called the surface plasmon absorption or plasmon resonance.[70] This plasmon band is influenced by the size and shape of the particles as well as the polydispersity, that is the range of particle sizes found in a sample, and this can be used as a diagnostic tool to characterise the particles. In general for a given shape, the wavelength of maximum absorbance, λ_{max}, shifts towards the red with increasing nanoparticle size.[70] The polydispersity of a sample, that is the distribution of sizes of nanoparticles, will affect the width of the plasmon band, with a greater polydispersity resulting in a broader absorption. The plasmon bands of Group 11 metals (copper, silver and gold) are unique among transition metals in that they are strong and narrow. Spherical silver particles absorb light with a wavelength of around 420 nm, giving rise to a golden-yellow coloured solution, while gold particles can absorb anywhere between 500 and 600 nm depending on shape, resulting in solutions ranging in colour from red to purple.[70]

Most particles require capping agents of some sort to stabilise them and prevent agglomeration. Without such ligands, particles show a tendency to form large aggregates. While it is possible to induce electrostatic repulsion between particles by

means of a layer of ions adsorbed on the surface of the particle, steric repulsion arising from adsorbed surfactants or polymers is most common.[74, 75] Cadmium selenide nanoparticles suspended in toluene are frequently stabilized with a layer of trioctylphosphine oxide (TOPO) ligands,[75] and long-chain alkyl thiols are commonly applied to gold nanoparticles.[76]

Existing photogeneration methods suffer from low efficiencies, requiring anything from tens of minutes to hours to produce appreciable quantities of nanoparticles.[67, 68] In addition, chemical precipitation methods require high temperatures to achieve the supersaturation necessary to precipitate nanoparticles.[77] A simple, efficient method for rapid nanoparticle generation under mild conditions is therefore highly desirable.

1.1.2 Magnetism

The phenomenon of magnetism arises from the movement of electrical charge,[78] In an electromagnet, that charge is the electric current moving through the wire. If the wire is bent into a loop, the magnetic field lines will point through the centre of the loop. If multiple turns of wire are wrapped around a block of iron, a powerful electromagnet is created, with the strength of the magnetic dipole being proportional to the applied current and number of loops in the wire.

In addition, magnetism can also arise from the spin of electrons in materials,[78] All materials exhibit some form of magnetism based on the magnetic moment of the

electrons in their atoms. Most materials exhibit diamagnetism, which is only evident in the presence of an externally applied magnetic field. This phenomenon is seen in materials having a negative magnetic susceptibility: for example, most organic substances, metals such as gold and silver and radicals in the singlet state. The response of the electrons to the applied field is to change their orbital motion, either speeding up or slowing down. The phenomenon seen on the macro scale is repulsion of the object or material from the source of the external field. This magnetic force is very weak compared to other forms of magnetism, but a sufficiently strongly applied field can cause levitation of a diamagnetic object.[79]

Materials with a positive magnetic susceptibility are called paramagnetic,[78] Paramagnetism is also seen only in the presence of an external field, but results in the attraction of the material toward the field source rather than repulsion. Paramagnetism arises mostly from the interaction of the applied field with the spin of unpaired electrons in metals such as aluminium or calcium, or in triplet species such as ground-state oxygen.

1.1.3 Zeeman Splitting

The Zeeman effect is the splitting of spectral absorbance bands in the presence of a magnetic field.[80] This is caused by degenerate energy sublevels interacting with the field in different ways. A triplet, for example, has three degenerate sublevels in the absence of a magnetic field, labeled T_+, T_0 and T_- with magnetic spin numbers of +1, 0 and –1 respectively.[ibid] The magnetic moments of these spins can be parallel, antiparallel

or perpendicular to the applied field. In the case of T_-, the spin is parallel to the field and as a result is stabilised. The opposite effect is seen in the case of the antiparallel T_+, being destabilized by the same amount that T_- is stabilised. T_0 is perpendicular to the field, and is not affected at all. It is important to note that the energy level of T_0 does not change in the magnetic field – it is the same as the triplet energy at zero field. The energetic separations of the triplet sublevels are typically in the radio or microwave range, depending on the strength of the magnetic field.

1.1.4. Magnetic Properties of Silver Nanoparticles

Being diamagnetic, silver nanoparticles display no inherent magnetism unless an external magnetic field is applied. When such a field is applied, however, the dipole interaction will cause the particles to repel each other. This can be used to synthesise ordered 2D arrays of nanoparticles on a solid substrate.[81] Arrays of silver nanoparticles can also be employed in the fabrication and study of magnetic nanostructures,[82] and the magnetic properties of nanoparticles in general are opening up new possibilities for media for data storage.[83, 84]

1.1.5. Previous Studies of Magnetic Field Effects of Ketyl Radicals

When benzophenone is photoexcited to the triplet state, it can abstract a hydrogen atom from a suitable donor, forming a geminate ground-state triplet radical pair consisting of a ketyl derived from benzophenone (BPK) and the corresponding radical derived from the donor (Scheme 1.2).[85] When confined in surfactant micelles, the lifetime of this state is longer compared to the same radical pair in homogeneous solution. This geminate state can be destroyed by one or both halves exiting the micelle, or by radical recombination through conversion to the singlet state. Because the singlet of this radical pair is close in energy to the triplet state radical pair, intersystem crossing and therefore radical recombination occurs very readily. When in solution, the radicals generally diffuse away from each other before this can occur. However, if the radicals are caged in micelles (for instance), they are confined in close proximity, and magnetic field effects can occur. Zeeman splitting of the degenerate triplet sublevels caused by an applied external magnetic field can raise and lower the T_+ and T_- sublevels respectively (Scheme 1.1). The third sublevel, T_0, is not affected. This loss of degeneracy is sufficient to shut off the recombination from these two sublevels, effectively reducing the efficiency of the process by up to two thirds.[85] Laser flash photolysis indicates that under these conditions, the ketyl radical is very long lived, on the order of microseconds as compared to hundreds of nanoseconds in the absence of a magnetic field. This increased lifetime enables one or both halves of the radical pair to exit the micelle more

efficiently and thereby increases the availability of the ketyl radical for non-geminate reactions.

Scheme 1.1. Zeeman splitting of the triplet sublevels by a magnetic field. T_0, T_+ and T_- are the sublevels of the ground-state triplet pair, S1 is the corresponding excited singlet state and H is the applied magnetic field.

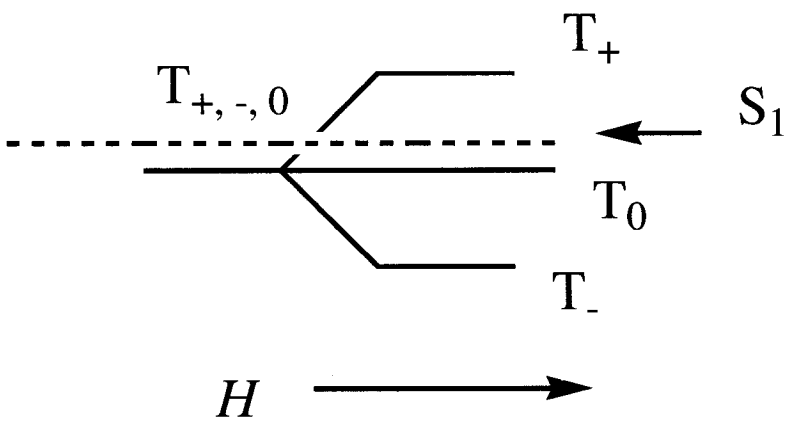

The photogeneration of metallic silver nanoparticles from benzophenone-derived ketyl radicals is described in Scheme 1.2.[67] The ketyl radicals formed from the abstraction of a hydrogen atom from 1,4-cyclohexadiene reduce Ag^+ to Ag^0. The enhanced lifetime of the ketyl radical as a result of the magnetic field effect should increase the rate of photogeneration of reduced silver and hence increase the rate of formation of silver nanoparticles. Evidence for this will be gathered by monitoring the characteristic plasmon absorbance around 420 nm.

Scheme 1.2. Mechanism of photogeneration of silver nanoparticles by benzophenone ketyl radicals

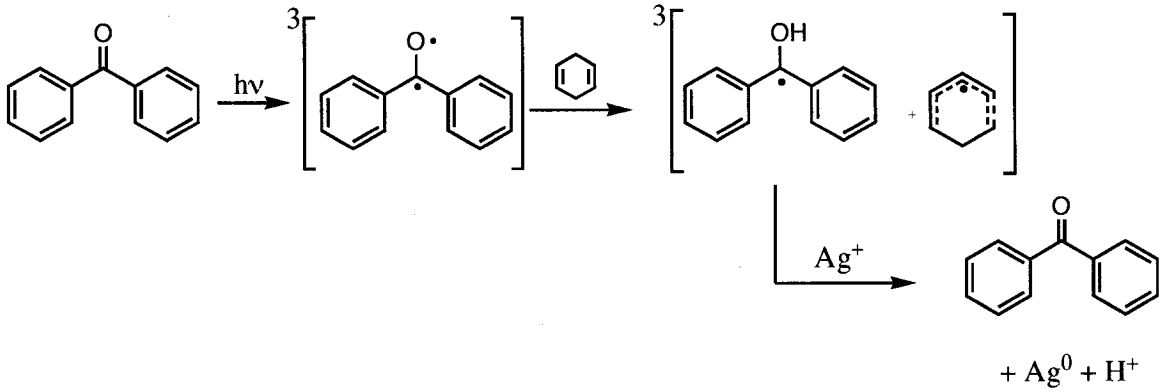

The purpose of this research is to investigate whether the known magnetic field effect on the lifetime of ketyl radicals can influence the rate of formation of silver nanoparticles.

1.2. Results

1.2.1. Triplet Benzophenone

Laser flash photolysis was also employed to determine the rate of quenching of the benzophenone triplet by Ag^+. By adding aliquots of 0.1 M $AgNO_3$ solution to the laser cell, the quenching rate constant was found to be 5.8 x 10^9 ± 6.4 x 10^8 M^{-1} s^{-1} in 0.1 M SDS micelles in aqueous solution (Figure 1.1). This quenching constant is close to the limit for diffusion control in water (7.4 x 10^9 $M^{-1}s^{-1}$ at 25°C).[86]

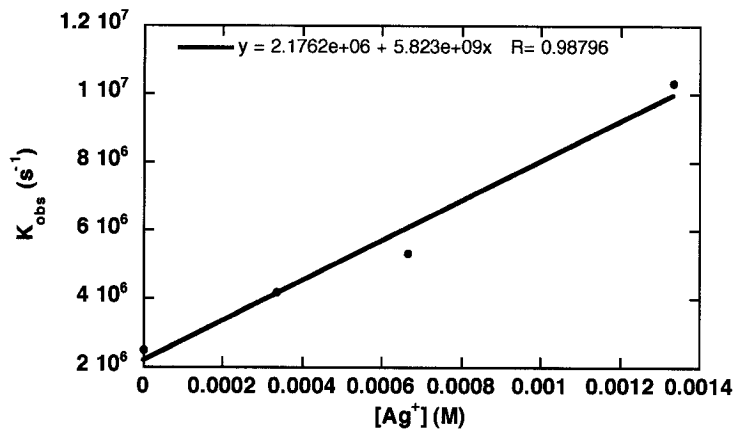

Figure 1.1: Observed decay rate constant of excited benzophenone triplet, $^3BP^*$, versus $[Ag^+]$ in SDS micelles in aqueous solution quenched by Ag^+. The system was excited at 355 nm and monitored at 530 nm. Solutions of 0.1 M SDS and 0.01 M BP were nitrogen-purged with a vortex mixer and silver was added from a 0.1 M $AgNO_3$ stock solution.

The excited spectrum of the benzophenone triplet displays a distinctive peak at 530 nm (Figure 1.2). This peak is quenched when 0.1 M of Ag^+ is added; the high concentration is employed to ensure complete quenching. The 530 nm peak of the benzophenone ketyl radical arising from reaction of the BP triplet with the SDS cage is also quenched (Figure 1.5).

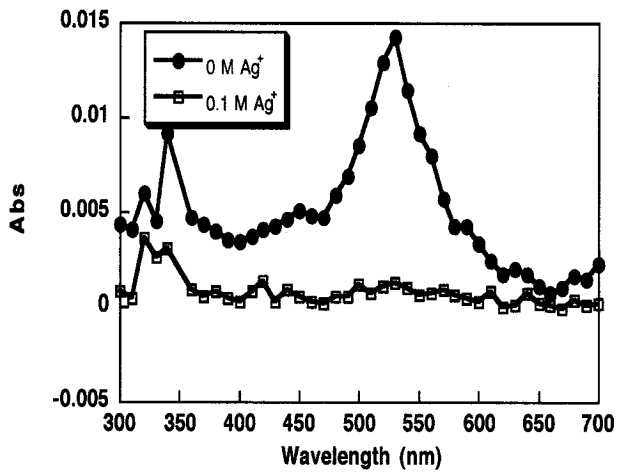

Figure 1.2: Transient absorbance spectra of benzophenone triplet with and without 0.1 M $AgClO_4$ from vortex-purged solutions of 0.1 M SDS and 0.01 M BP and excited at 355 nm. Spectra were acquired 1.20 μs after the laser pulse.

1.2.2. Magnetic field effects on Benzophenone Ketyl Radicals

Laser flash photolysis was used to monitor the lifetimes of the benzophenone ketyl radical in the absence and presence of a magnetic field. Both the ketyl radical and the triplet of benzophenone absorb at 530 nm,[85] but the triplet state also absorbs at 600 nm. While this triplet signal is not as strong as that at 530 nm, it does have the advantage

of being unique to the triplet state and not subject to interference from the ketyl radical. This signal can be used to verify that the triplet is short lived in the presence of 1,4-CHD. In the absence of a magnetic field, the ketyl radical absorption returns approximately to 15% of the maximum ΔO.D. (Figure 1.3). When a magnetic field of 100mT is applied, the long-lived ketyl radical persists for hundreds of nanoseconds (Figure 1.4). The transient spectrum (Figure 1.5) shows a distinctive peak at 530 nm. This peak is not completely quenched by Ag^+ under experimental conditions of nanoparticle formation; only two thirds of the ketyl radicals are trapped by the silver cations in the timescale under consideration – it seems likely that they would all be quenched at longer timescales.

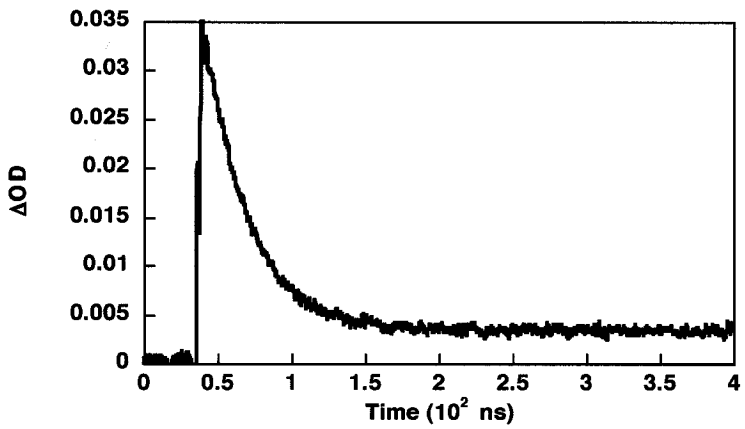

Figure 1.3: Transient absorbance decay trace of the benzophenone ketyl radical in SDS micelles in aqueous solution excited at 355 nm and monitored at 530 nm in a 0 mT magnetic field from vortex-purged solutions of 0.1 M SDS, 0.01 M BP and 0.04 M 1,4-CHD.

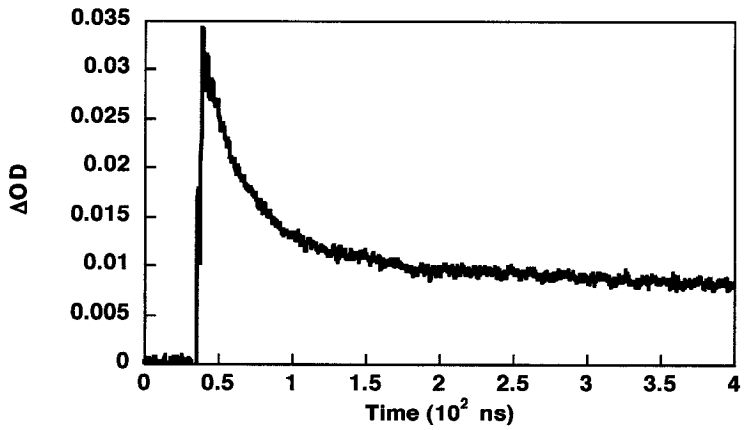

Figure 1.4: Transient absorbance decay trace of the benzophenone ketyl radical in SDS micelles in aqueous solution excited at 355 nm and monitored at 530 nm in a 100 mT magnetic field from vortex-purged solutions of 0.1 M SDS, 0.01 M BP and 0.04 M 1,4-CHD.

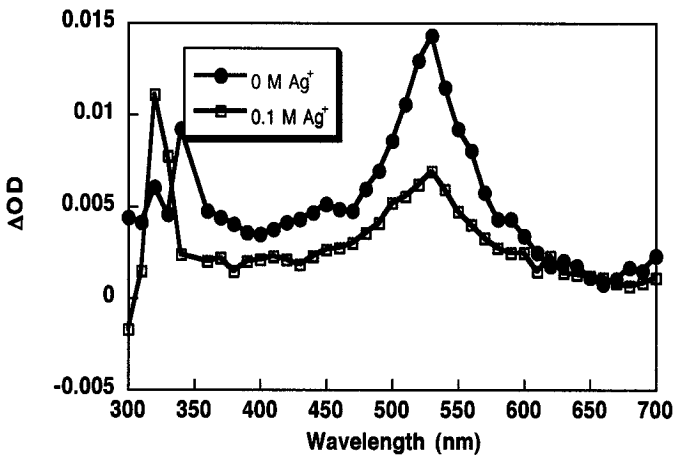

Figure 1.5: Transient absorbance spectra of benzophenone ketyl radical with and without 0.1 M $AgClO_4$ from vortex-purged solutions of 0.1M SDS, 0.01M BP and 0.04 M 1,4-CHD and excited at 355 nm. Spectra were acquired 1.20 μs after the laser pulse.

1.2.3. Photogeneration of Silver Nanoparticles in Micelles

When samples containing 0.1 M SDS, 0.005 M BP, 0.01M $AgNO_3$ and 0.04 1,4-CHD are irradiated for 30 seconds with a Xenon lamp employing a 320 nm cutoff filter, a plasmon absorbance band appears at 412 nm. This spectrum also contains an absorbance band at ~350 nm arising from the n-π transition of benzophenone. Since the source of this band is present before and after irradiation, it can be subtracted from the irradiated spectrum, yielding a clean plasmon band (Figure 1.6).

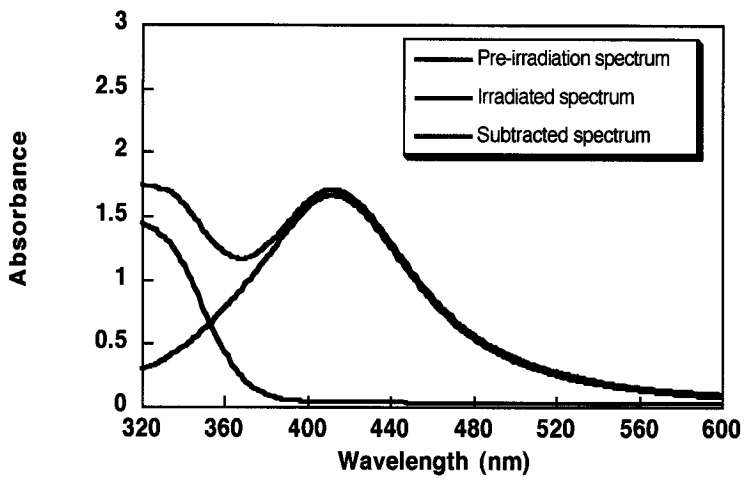

Figure 1.6: Plot of absorbance spectra of silver nanoparticles showing the subtraction of the pre-irradiation spectra. Particles were photogenerated from solutions of 0.1 M SDS, 0.005 M BP and 0.04 M 1,4-CHD following vortex purging with nitrogen and 30 seconds irradiation with an Oriel Xenon lamp and 320 nm cutoff filter.

1.2.4. Stability of Silver Nanoparticles

Organic solvents were used in an attempt to extract the nanoparticles from the aqueous phase, but no yellow colour was obser*ved in the organic layers, while the aqueous layer turned dark brown almost instantaneously upon agitation. Samples of 3 mL were prepared without magnetic field exposure and extracted in a separatory funnel with approximately equal volumes of solvent (Figure 1.7). The plasmon band broadened considerably for each solvent (Figure 1.8) due to aggregation of the nanoparticles, although the change in absorbance intensity varied considerably, decreasing slightly in diethyl ether, substantially in chloroform and increasing slightly in cyclohexane. The λ_{max} shifted to longer wavelengths for every solvent, most drastically for diethyl ether. In addition, the benzophenone absorption band at 325 nm decreases for all solvents, as expected, since benzophenone should be extracted into the organic phase.

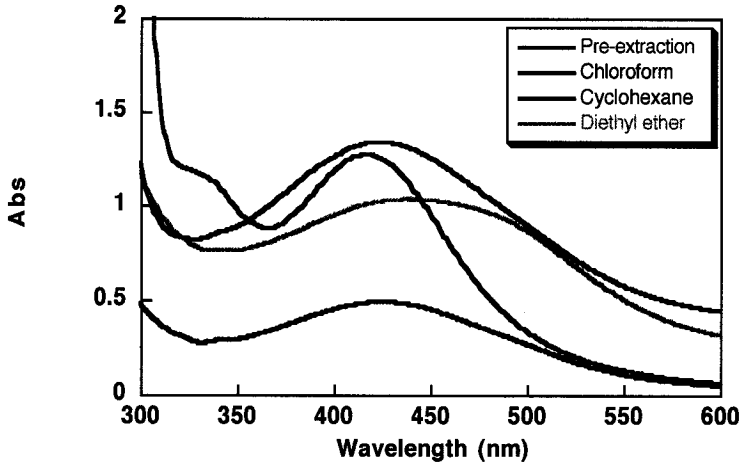

Figure 1.7: Absorbance spectra of the aqueous phase of silver nanoparticles before and after extraction by various solvents from a solution of 0.1 M SDS, 0.005 M BP, 0.04 M 1,4-CHD and 0.01 M $AgNO_3$ following vortex purging with nitrogen and 30 seconds irradiation with an Oriel Xenon lamp and 320 nm cutoff filter.

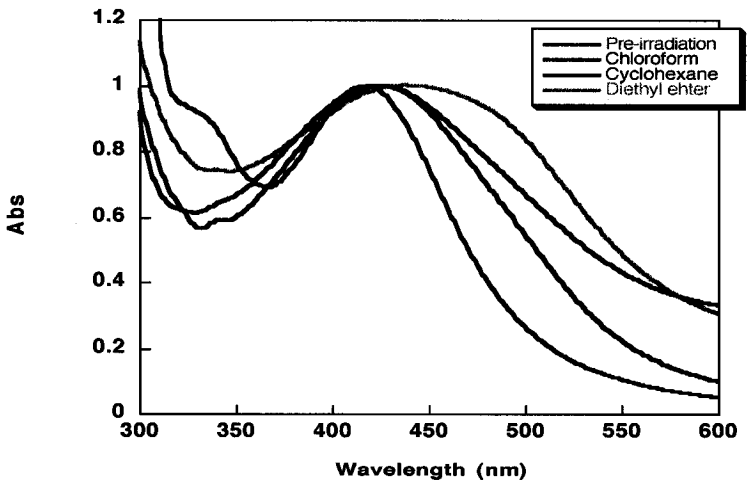

Figure 1.8: Absorbance spectra from Figure 1.7 normalised to λ_{max} to show effects of solvent extraction on peak width. Experimental conditions are the same as Figure 1.7.

An infrared spectrum of the Ag1,4-CHD complex did not display any peaks distinctive to 1,4-CHD (Figure 1.9). The only peak visible at 1300 cm^{-1} is attributed to the N=O stretch in NO_3^-. Samples were prepared by mixing 0.01 M $AgNO_3$ and 0.04 M 1,4-CHD in acetonitrile and then pipetting over a salt plate and allowing the solvent to evaporate. A strong odour of 1,4-CHD was noted during this process.

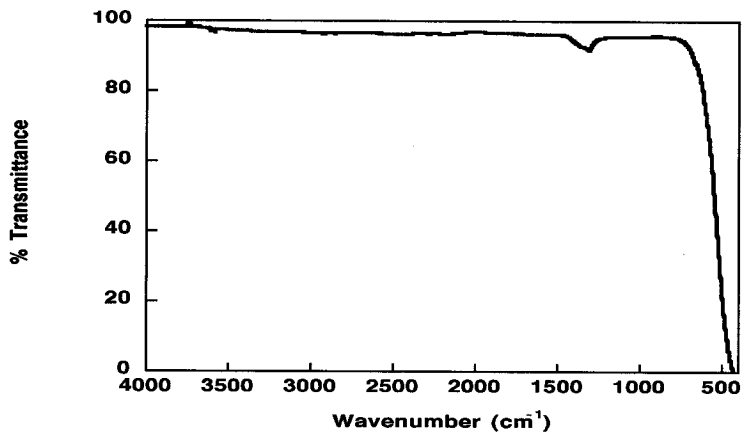

Figure 1.9: Infrared spectrum of non-irradiated 0.01 M $AgNO_3$ and 0.04 M 1,4-CHD dissolved in ACN. Samples were prepared by pipetting the solution over NaCl salt plates and allowing the solvent to evaporate. The baseline spectrum was that of dried air from a purge gas generator, and the spectrum was acquired in an atmosphere that had been passed through a desiccant.

When 1 mL of methanol was added to a 3 mL irradiated solution containing 0.1 M SDS, 0.005M BP, 0.01M Ag^+ and 0.04 M CHD and allowed to mix, the intensity of

plasmon absorbance band was halved from 1.6 to 0.8. In addition, the peak broadened considerably and the maximum absorbance shifted from 414 nm to 436 nm.

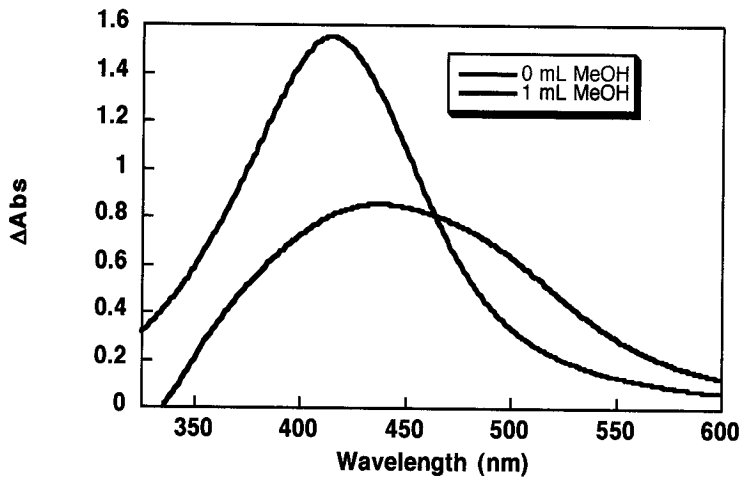

Figure 1.10: Absorbance spectra of silver nanoparticles showing the effect of added methanol. Particles were photogenerated from solutions of 0.1 M SDS, 0.005 M BP, 0.04 M 1,4-CHD and 0.01 M $AgNO_3$ following vortex purging with nitrogen and 30 seconds irradiation with an Oriel Xenon lamp and 320 nm cutoff filter, with 1 mL of MeOH subsequently injected through the septum. All spectra have had the pre-irradiation absorbance subtracted.

1.2.5. The Effect of Silver Ion Concentration on Nanoparticle Formation

In light of the quenching of benzophenone triplet by silver(I), it is important to determine the effects of variations in concentration on the generation of nanoparticles. Reducing the concentration of silver ions from 10 mM to 5 mM has the effect of increasing the rate of production of nanoparticles, as indicated by the plasmon band

intensity (Figure 1.11). As the concentration of silver is increased above 10 mM, the plasmon intensity decreases and the band becomes broader in a manner consistent with aggregation of particles. This phenomenon is illustrated by plotting normalised absorbance spectra (Figure 1.12).

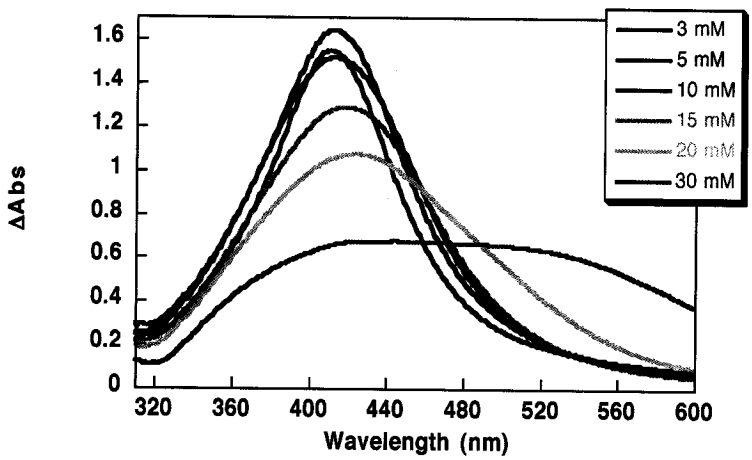

Figure 1.11: Plot of absorbance spectra of silver nanoparticles at various Ag^+ concentrations in solutions of 0.1 M SDS, 0.005 M BP and 0.04 M 1,4-CHD following vortex purging with nitrogen and 30 seconds irradiation with an Oriel Xenon lamp and 320 nm cutoff filter. All spectra have had the pre-irradiation absorbance subtracted.

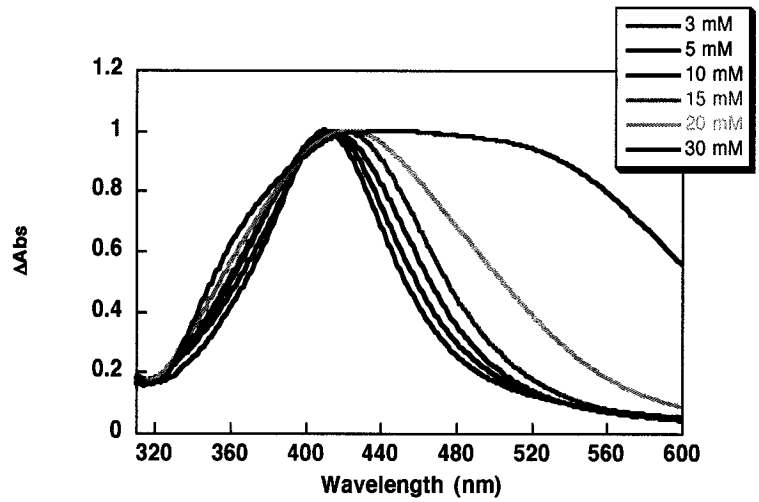

Figure 1.12: Absorbance spectra from Figure 1.11 normalised to λ_{max} to show effect of changes in $[Ag^+]$ on peak broadness. Experimental conditions are the same as Figure 1.11.

1.2.6. The Effect of 1,4-CHD on Nanoparticle Formation

1,4-cyclohexadiene (1,4-CHD) acts as a hydrogen donor in the formation of the ketyl radical from benzophenone. Samples with CHD showed a substantial increase in plasmon band formation compared to samples without it (Figure 1.13). In addition, the plasmon bands of silver nanoparticles formed in the presence of CHD were generally both narrower and more symmetrical. When the 1,4-CHD concentration was decreased from 40 mM to 10 mM, the plasmon band broadened and developed a long tail at longer wavelengths (Figure 1.18).

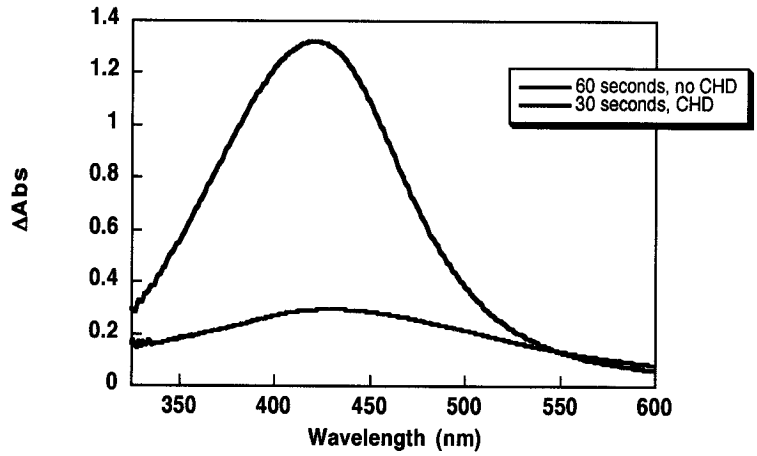

Figure 1.13: Plot of absorbance spectra of silver nanoparticle plasmon bands with and without 1,4-CHD present throughout irradiation for solutions of 0.1 M sodium dodecyl sulphate, 0.005 M benzophenone, 0.04 M 1,4-cyclohexadiene and 0.01 M Ag NO_3 following vortex purging with nitrogen. Irradiation was carried out with an Oriel Xenon lamp and a 320 nm cutoff filter. Pre-irradiation spectra have been subtracted.

Addition of 1,4-CHD to the solution with typical reaction conditions after irradiation appeared to stabilise the particles (Figure 1.15). After five hours, during which time the samples were kept wrapped in aluminium foil in the dark, the spectrum of the sample with 1,4-CHD showed a shorter λ_{max} and a less unsymmetrical tail, although the intensity of the plasmon absorbance had decreased slightly. The sample without 1,4-CHD, on the other hand, showed an increase in the tail between 500 and 600 nm. After 72 hours, the spectrum of the sample with 1,4-CHD was still relatively narrow and the plasmon band intensity had actually increased beyond its initial absorbance. The other sample increased as well across the whole spectrum, most dramatically between 500 and

600 nm. A distinct shoulder developed at about 550 nm. These changes can be seen in Figure 1.16. Visually, the sample without 1,4-CHD changed from an initial light brown to a dark brown, as compared to the golden-yellow colour that developed in the sample with 1,4-CHD added after irradiation (Figure 1.14). Note that a much stronger LuzChem lamp was used for this experiment instead of the usual Oriel lamp because of the temporary unavailability of the Oriel unit.

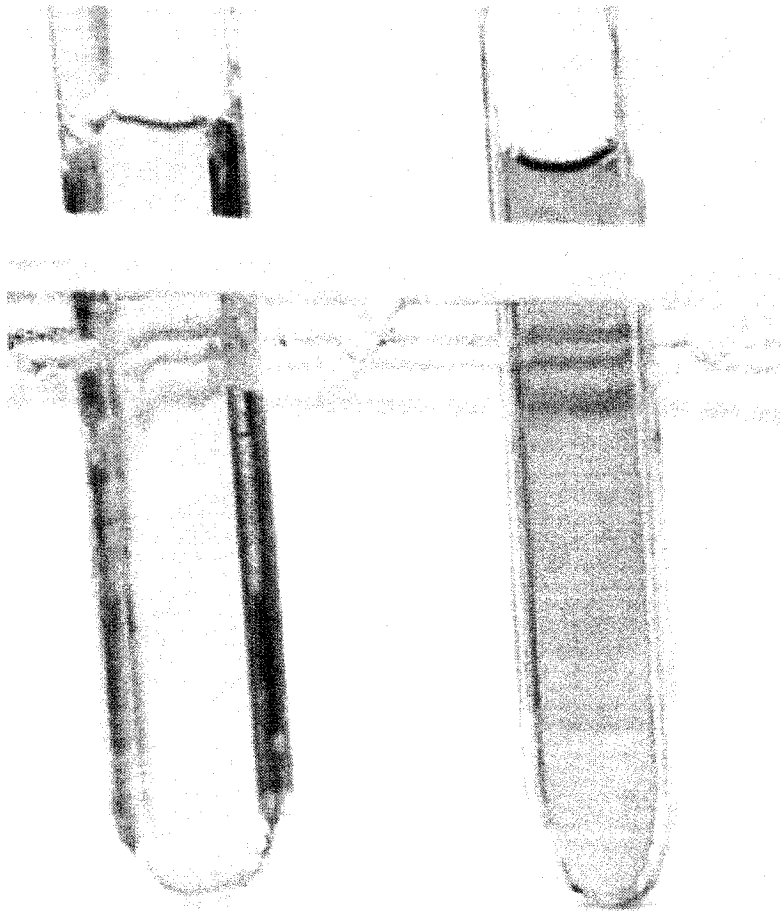

Figure 1.14: Photograph of silver nanoparticle solutions. Solutions contain 0.1 M sodium dodecyl sulphate, 0.005 M benzophenone, 0.01 M $AgNO_3$ and were vortex-purged prior to irradiation. 0.04M 1,4-CHD was injected through the septum of the cuvette on the left immediately after 5 seconds irradiation with a LuzChem Xenon lamp and a 320 nm cutoff filter. Photo taken 24 hours after irradiation.

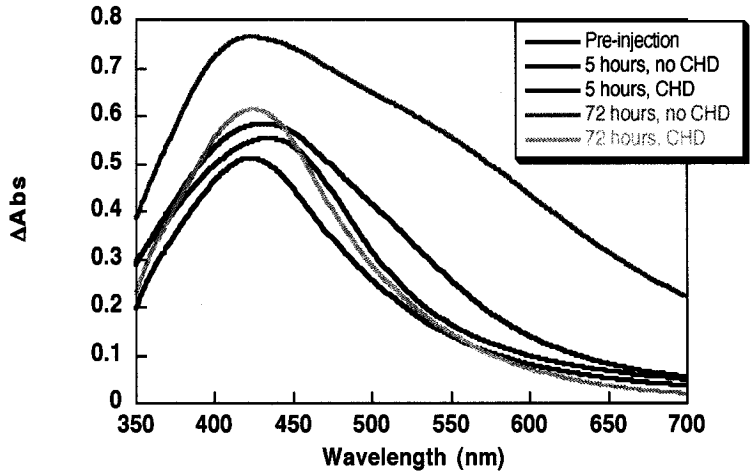

Figure 1.15: Absorbance spectra of silver nanoparticle plasmon bands with and without 0.04 M 1,4-CHD added after irradiation. Solutions of 0.1 M sodium dodecyl sulphate, 0.005 M benzophenone, 0.01 M $AgNO_3$ were vortex-purged prior to irradiation. 0.04 M 1,4-CHD was injected through the septa immediately after 5 seconds irradiation with a LuzChem Xenon lamp and a 320 nm cutoff filter.

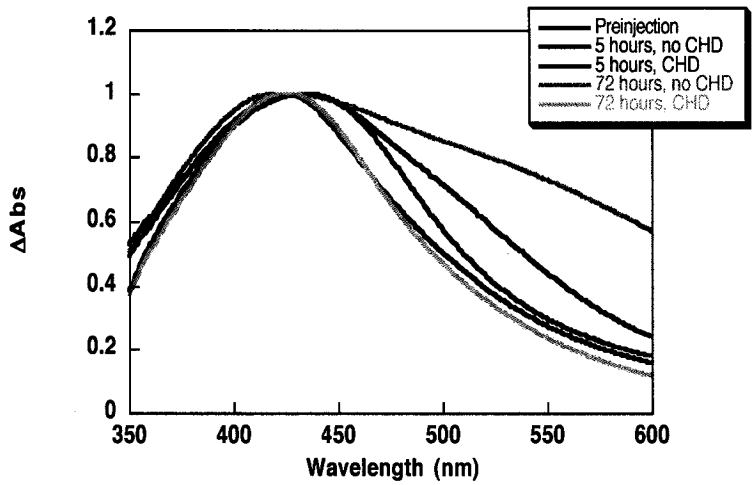

Figure 1.16: Absorbance spectra from Figure 1.15 normalised to λ_{max} to show effects of 1,4-CHD stabilisation on peak width. Experimental conditions are the same as Figure 1.15.

The absorbance of the plasmon band without 1,4-CHD injected increased linearly over time, but the absorbance of the sample with 1,4-CHD initially decreased before increasing again to approximately the same intensity of the sample without CHD after 95 hours (Figure 1.17).

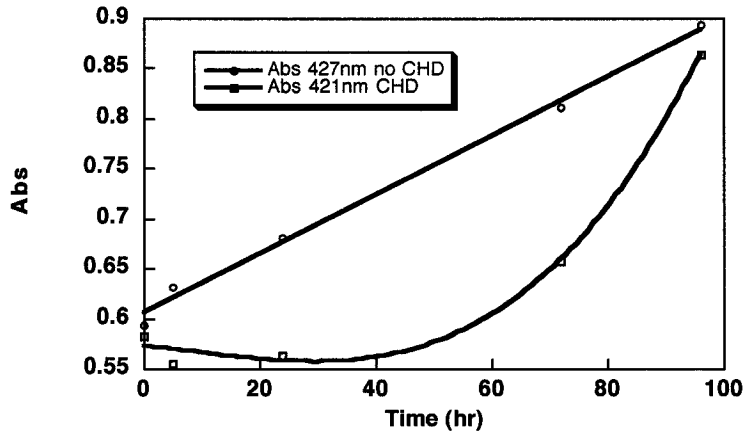

Figure 1.17: Maximum absorbance of plasmon bands from Figure 1.15 with respect to time after irradiation, with and without 1,4-CHD added. Experimental conditions are the same as Figure 1.15.

An increase in the concentration of 1,4-CHD resulted in a corresponding increase in the absorbance of the plasmon band, but the full width half maximum (fwhm) was not as dramatically affected as it was by changes in the concentration of Ag^+ (Figure 1.18). As [1,4-CHD] increases, the plasmon band becomes narrower (Figure 1.19).

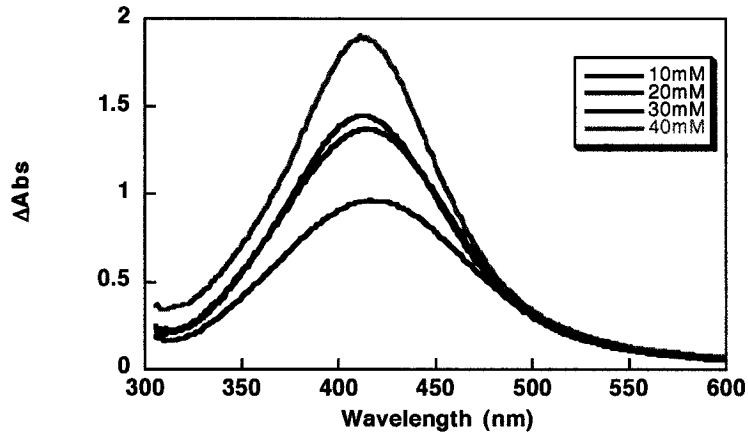

Figure 1.18: Plot of absorbance spectra of silver nanoparticles with various 1,4-CHD concentrations added prior to irradiation. Solutions of 0.1 M sodium dodecyl sulphate, 0.005 M benzophenone, 0.04 M 1,4-cyclohexadiene and 0.01 M $AgNO_3$ were vortex-purged prior to 30 seconds irradiation with an Oriel Xenon lamp and 320 nm cutoff filter. Pre-irradiation spectra have been subtracted.

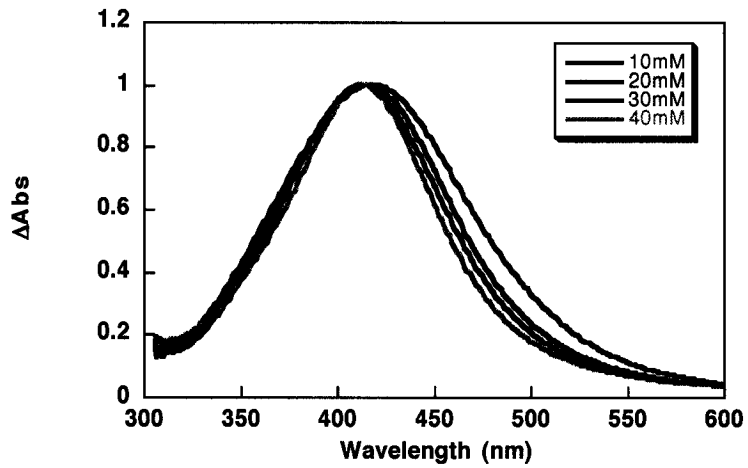

Figure 1.19: Absorbance spectra from Figure 1.18 normalised to λ_{max} to show effects of variations in [1,4-CHD] on peak width. Experimental conditions are the same as Figure 1.18.

1.2.7. Effect of Magnetic Fields on the Photogeneration of Nanoparticles by Benzophenone Ketyl Radicals

Ultraviolet-visible absorption spectroscopy was used to monitor the plasmon band formation, before and after nanoparticle formation. When a magnetic field was applied during irradiation of the sample containing 0.1 M SDS, 0.005 M benzophenone, 0.01M $AgNO_3$ and 0.04M 1,4-CHD, the plasmon band intensity showed a dramatic increase over samples unexposed (Figure 1.20). This dramatic increase upon 30 seconds irradiation in a magnetic field appeared even with a relatively weak field of 25 mT. Increasing the magnetic field strength caused additional increases in the plasmon band up to 75 mT. Increasing the magnetic field strength from 75 mT to 125 mT did not increase the plasmon band intensity appreciably (Figure 1.21).

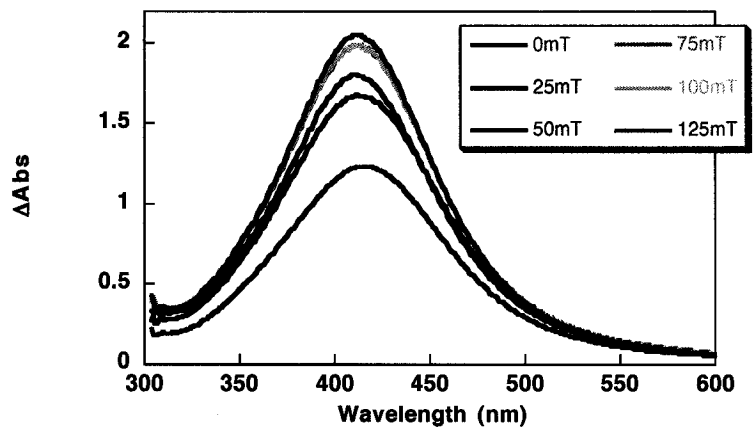

Figure 1.20: Plot of absorbance of silver nanoparticles. Spectra of solutions of 0.1 M sodium dodecyl sulphate, 0.005 M benzophenone, 0.04 M 1,4-cyclohexadiene and 0.01 M $AgNO_3$ following vortex purging with nitrogen and 30 seconds irradiation with an Oriel Xenon lamp and 320 nm cutoff filter. All spectra have had the pre-irradiation absorbance subtracted.

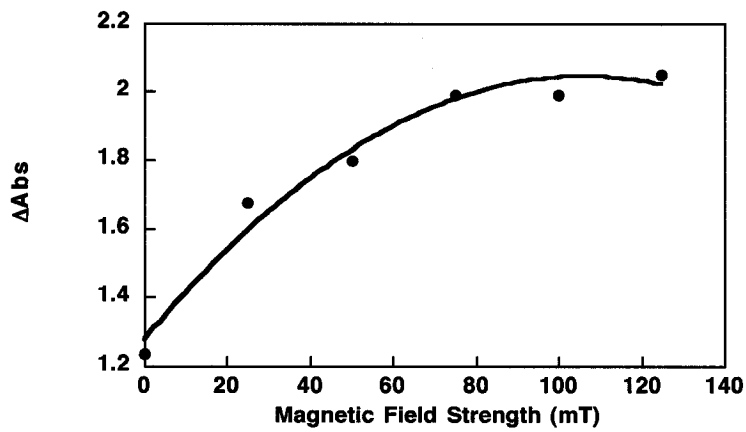

Figure 1.21: Plot of plasmon band absorbance versus magnetic field strength at 420 nm for solutions of 0.1 M sodium dodecyl sulphate, 0.005 M benzophenone, 0.04 M 1,4-cyclohexadiene and 0.01 M $AgNO_3$ following vortex purging with nitrogen and 30 seconds irradiation with an Oriel Xenon lamp and 320 nm cutoff filter. The pre-irradiation absorbance values have been subtracted from all data points.

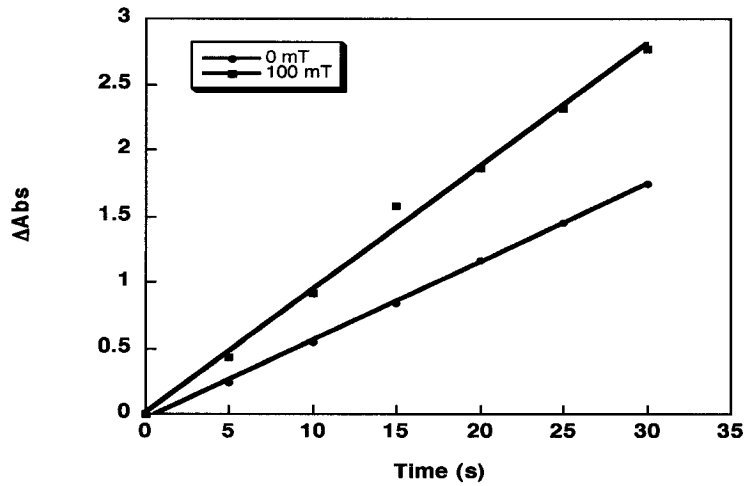

Figure 1.22: Absorbance of silver nanoparticle plasmon band at 420 nm with respect to irradiation time in the presence and absence of a magnetic field for solutions of 0.1 M sodium dodecyl sulphate, 0.005 M benzophenone, 0.04 M 1,4-cyclohexadiene and 0.01 M $AgNO_3$ following vortex purging with nitrogen and 30 seconds irradiation with an Oriel Xenon lamp and 320 nm cutoff filter. The pre-irradiation absorbance values have been subtracted from all data points.

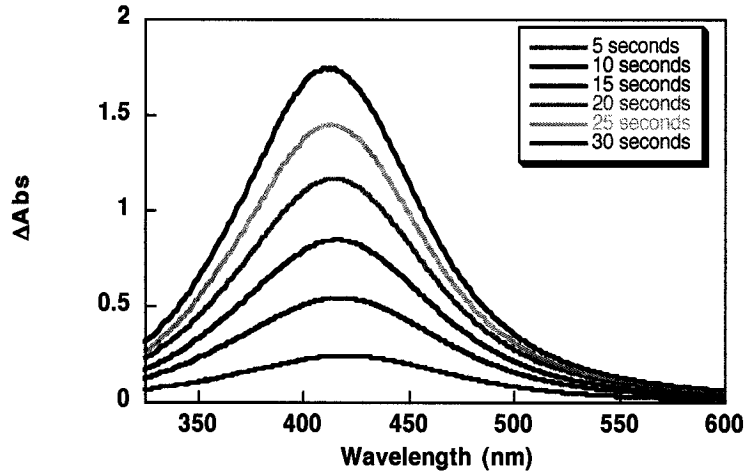

Figure 1.23: Absorbance spectra of silver nanoparticles at successive irradiation times showing the formation of the plasmon band at 0 mT magnetic field for solutions of 0.1 M sodium dodecyl sulphate, 0.005 M benzophenone, 0.04 M 1,4-cyclohexadiene and 0.01 M $AgNO_3$ following vortex purging with nitrogen and 30 seconds irradiation with an Oriel Xenon lamp and 320 nm cutoff filter. All spectra have had the pre-irradiation absorbance subtracted.

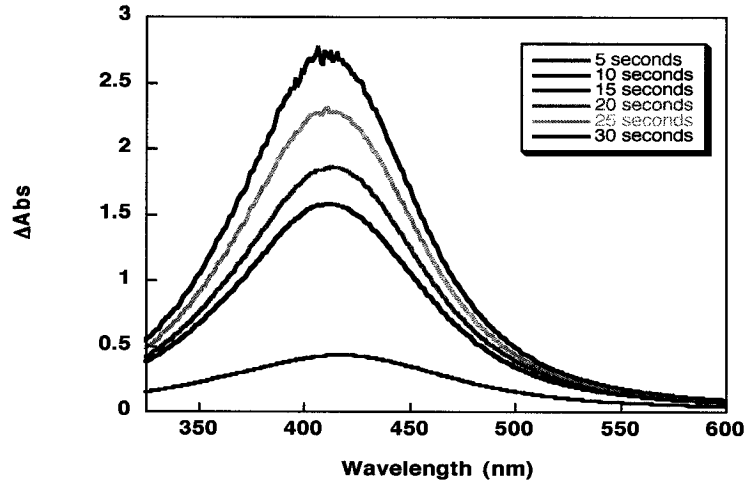

Figure 1.24: Absorbance spectra of silver nanoparticles at successive irradiation times showing the formation of the plasmon band at 100 mT magnetic field for solutions of 0.1 M sodium dodecyl sulphate, 0.005 M benzophenone, 0.04 M 1,4-cyclohexadiene and 0.01 M $AgNO_3$ following vortex purging with nitrogen and 30 seconds irradiation with an Oriel Xenon lamp and 320 nm cutoff filter. All spectra have had the pre-irradiation absorbance subtracted.

The plasmon absorbance bands grow-in steadily with increasing irradiation time (Figure 1.22). Samples were irradiated for 5-second increments and then removed from the apparatus so that absorbance spectra could be measured. During this time the cuvettes were kept wrapped in aluminium foil to minimize exposure to ambient lighting. The colour remained stable between irradiations while the sample was transferred to the spectrophotometer and the spectra were acquired. A slight (< 10 nm) shift in λ_{max} towards shorter wavelengths is observed with and without a 100 mT magnetic field, although the shift is more pronounced without the magnetic field. Without the magnetic field, λ_{max} shifts from 420 nm after 5 seconds of irradiation to 412 nm after 30 seconds

(Figure 1.23). With the magnetic field, these values are 415 nm and 410 nm (Figure 1.24). In addition, the plasmon bands generated in the magnetic field tend to be at shorter wavelengths than the corresponding plasmon bands generated without.

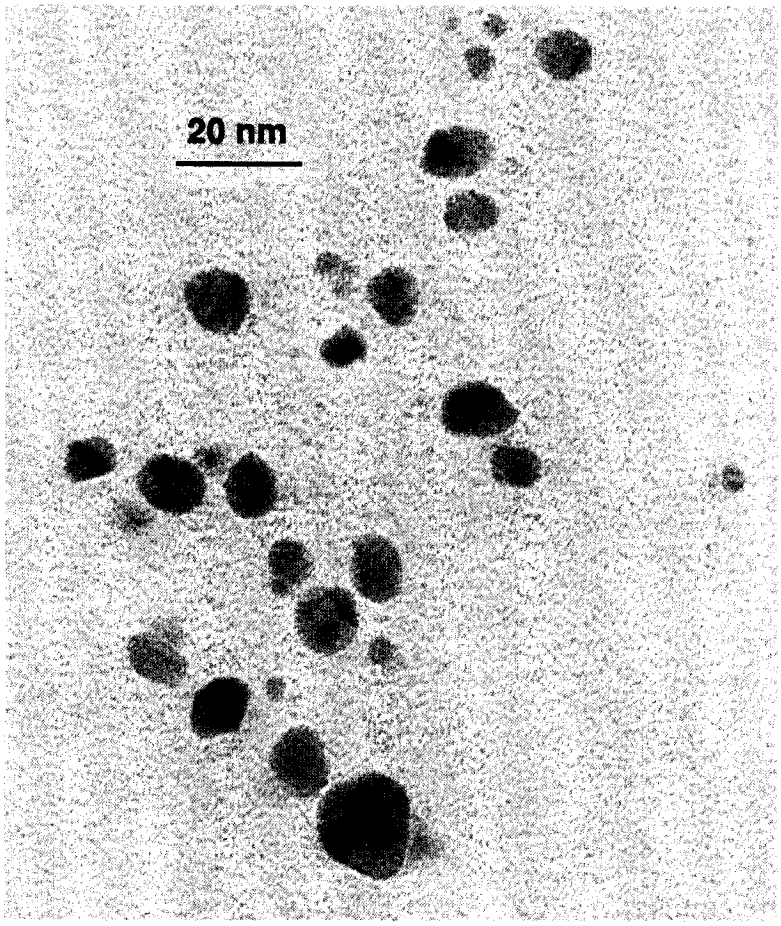

Figure 1.25: TEM images of washed silver nanoparticles photogenerated in a BP/SDS system with 1,4-CHD in the absence of a magnetic field from solutions of 0.1 M sodium dodecyl sulphate, 0.005 M benzophenone, 0.04 M 1,4-cyclohexadiene and 0.01 M $AgNO_3$ following vortex purging with nitrogen and 30 seconds irradiation with an Oriel Xenon lamp. 10 μL of solution was transferred by pipette to a 300 mesh carbon-coated copper TEM grid and then washed with MeOH. Image acquired at 200 kV.

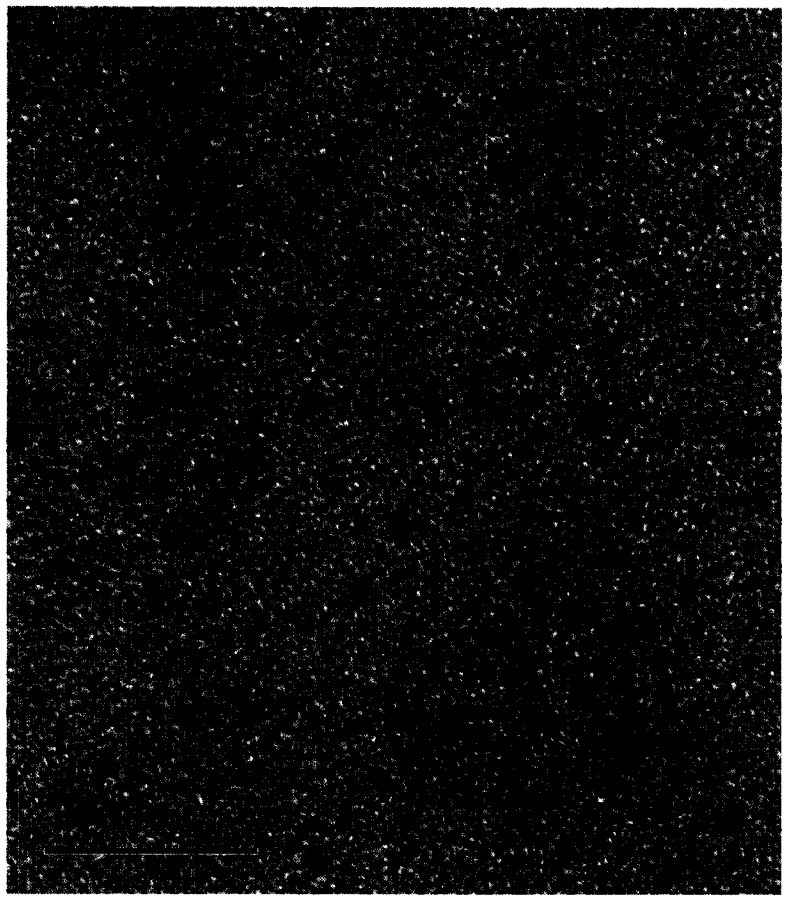

Figure 1.26: TEM images of unwashed silver nanoparticles photogenerated in a BP/SDS system with 1,4-CHD in the absence of a magnetic field from solutions of 0.1 M sodium dodecyl sulphate, 0.005 M benzophenone, 0.04 M 1,4-cyclohexadiene and 0.01 M $AgNO_3$ following vortex purging with nitrogen and 30 seconds irradiation with an Oriel Xenon lamp. The volume of solution was 10 μL, transferred by pipette to a 300 mesh carbon-coated copper TEM grid and not washed with MeOH. Image acquired at 200 kV.

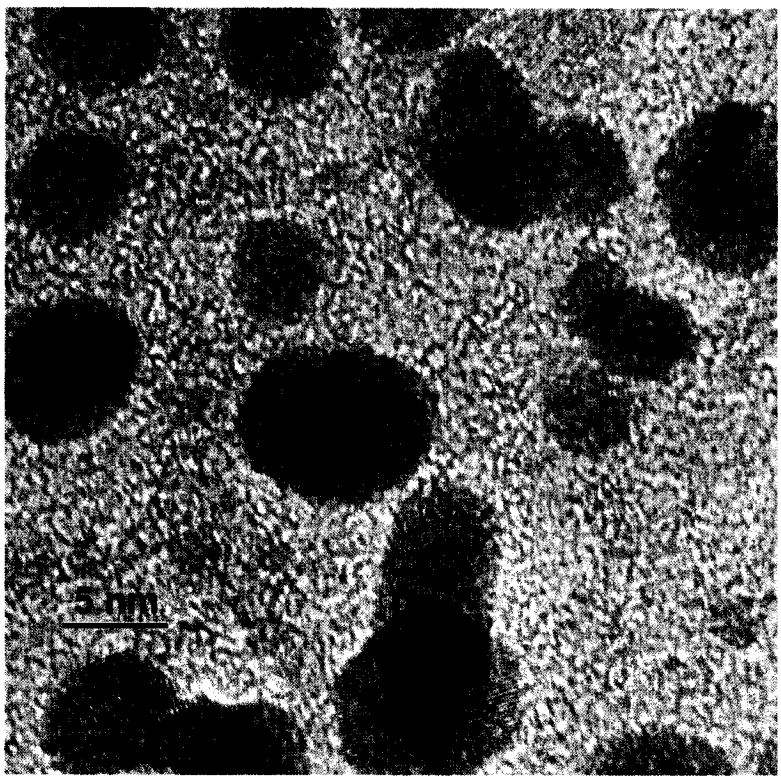

Figure 1.27: TEM images of particles photogenerated in a BP/SDS system with 1,4-CHD in a 6.34 mT magnetic field from solutions of 0.1 M sodium dodecyl sulphate, 0.005 M benzophenone, 0.04 M 1,4-cyclohexadiene and 0.01 M $AgNO_3$ following vortex purging with nitrogen and 30 seconds irradiation with an Oriel Xenon lamp. The volume of solution was 10 μL, transferred by pipette to a 300 mesh carbon-coated copper TEM grid and then washed with MeOH. Image acquired at 200 kV.

TEM imaging indicates that these particles are discrete, although washing with methanol causes dispersed particles to form loose aggregations (Figure 1.25). While most particles are approximately spherical, individual particles display tetrahedral morphologies. Most particles are polycrystalline - that is, each nanoparticle is divided into domains wherein the crystal axes are not in alignment with other domains (Figure

1.27). However, the hexagonal crystal visible at the very bottom of Figure 1.27 appears to be monocrystalline. The magnetic field effect caused a 60% increase in the size of the particles, resulting in particles with diameters of approximately 8 nm as compared to 5 nm for particles formed without the field (Figure 1.28).

One sample of particles formed with 1,4-CHD was not washed with MeOH during preparation. The image obtained from this sample (Figure 1.26) shows unaggregated particles, while the corresponding MeOH-washed sample (Figure 1.25) shows distinct clustering. The darker background in Figure 1.26 is due to the presence of organic material (SDS and BP) on the particles. The samples from which the images in Figures 1.25 and 1.26 were acquired were prepared from the same nanoparticle solution, so it seems likely that the apparent disparity in sizes noted between the two images is due to interference of the organic material.

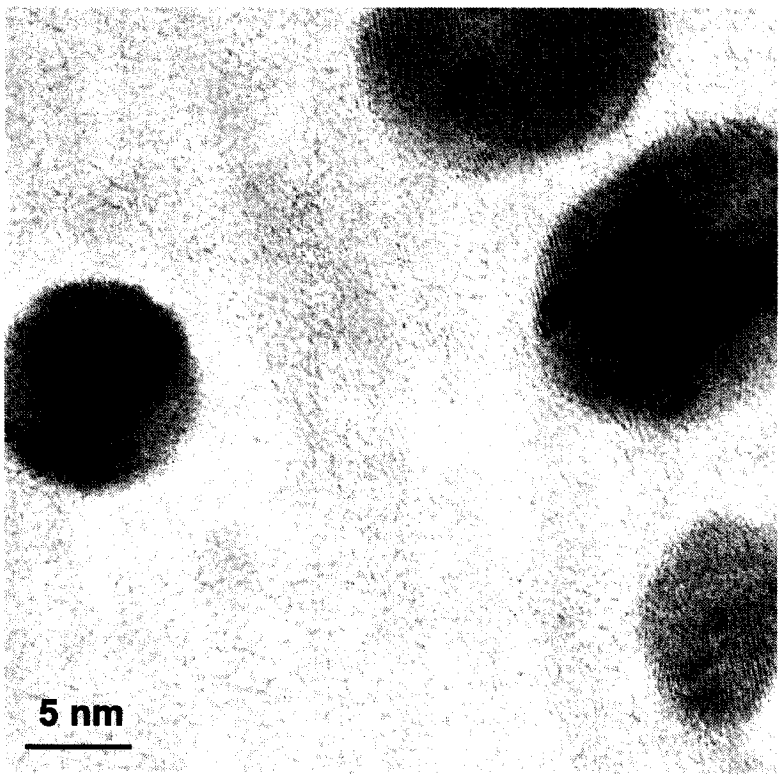

Figure 1.28: TEM images of particles photogenerated in a BP/SDS system with 1,4-CHD in a 15.6 mT magnetic field from solutions of 0.1 M sodium dodecyl sulphate, 0.005 M benzophenone, 0.04 M 1,4-cyclohexadiene and 0.01 M $AgNO_3$ following vortex purging with nitrogen and 30 seconds irradiation with an Oriel Xenon lamp. The volume of solution was 10 μL, transferred by pipette to a 300 mesh carbon-coated copper TEM grid and then washed with MeOH. Image acquired at 200 kV.

1.2.8. Effects of Benzhydrol as a Hydrogen Donor

Benzhydrol (diphenylmethanol) was chosen to replace 1,4-CHD as the hydrogen donor to examine the effects on nanoparticle formation of a radical pair in which both halves of the pair were identical radicals. The plasmon bands resulting from the reduction of silver generated by ketyl radicals generated from the reaction of benzhydrol

with benzophenone were very broad and required a longer irradiation time to achieve appreciable absorption (Figure 1.29). The magnetic field effect was less dramatic than in the BP-1,4-CHD system, showing an increase of about 45% at 125 mT (Figure 1.30). From the absence of a plateau region in the curve, it seems likely that nanoparticle production continues to increase above 125 mT, the highest field strength attainable by our instrumental setup.

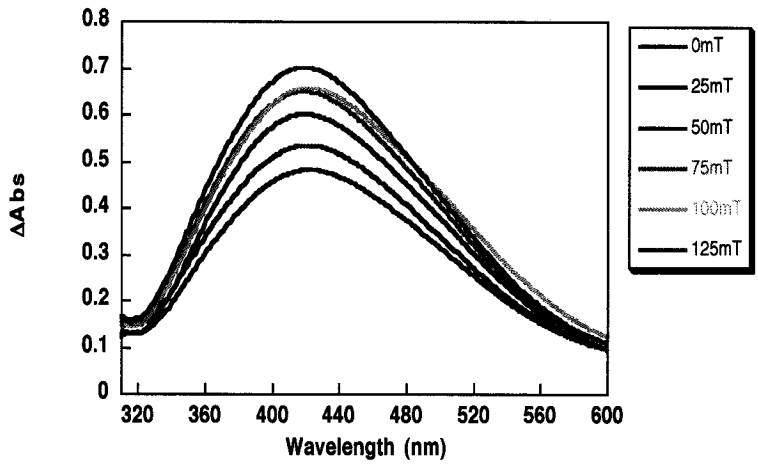

Figure 1.29: Plot of absorbance spectra of silver nanoparticles photogenerated from ketyl radicals derived from benzophenone and benzhydrol in solutions of 0.1 M SDS, 0.005 M BP, 0.02 M benzhydrol, 0.01 M $AgNO_3$ following vortex purging with nitrogen and 60 seconds of irradiation with an Oriel Xenon lamp and 320 nm cutoff filter. Pre-irradiation spectra have been subtracted.

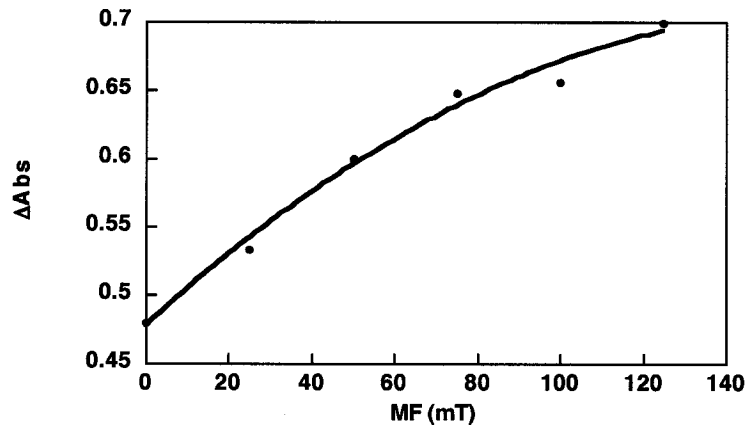

Figure 1.30: Plot of absorbance of plasmon band at 420 nm versus magnetic field strength at for nanoparticles generated by ketyl radicals derived from benzophenone and benzhydrol. Experimental conditions are the same as Figure 1.29.

1.2.9. Effects of Cationic Micelles on the Photogeneration and Stability of Ag Nanoparticles

Due to the hydrophobicity of benzophenone, micelles are required to solubilise it in aqueous solution. To determine whether the charge of these micelles played a role in the formation of nanoparticles, cationic cetyltrimethylammonium-based micelles were selected. The commercially available forms of this surfactant have bromide and chloride as counterions. Given the insolubility of Ag^+ with these anions, the nitrate form was prepared and used instead. The solubility of cetyltrimethylammonium nitrate (CTAN, prepared from CTAB or CTAC, see Experimental section) in water is less than that of SDS. As a result, a concentration of 0.1 M was not attainable, and a concentration of

0.025 M was used instead. The absorption of the Ag plasmon band after 30 seconds of irradiation was substantially less than that seen in SDS, 0.8 at 0 mT versus 1.2 (Figure 1.31). Magnetic field effects were seen with this system on a comparable scale to SDS micelles (Figure 1.32). However, the increase of the plasmon absorbance intensity with respect to magnetic field strength does not reach a plateau, and only shows a 32% increase at 125 mT. At first glance it appears that the degree of aggregation is much greater, even with 1,4-CHD present. Upon closer inspection, it is evident that there is a very weak overlapping peak at around 500 nm, and an isosbestic point is evident at about 460 nm for fields up to 75 mT.

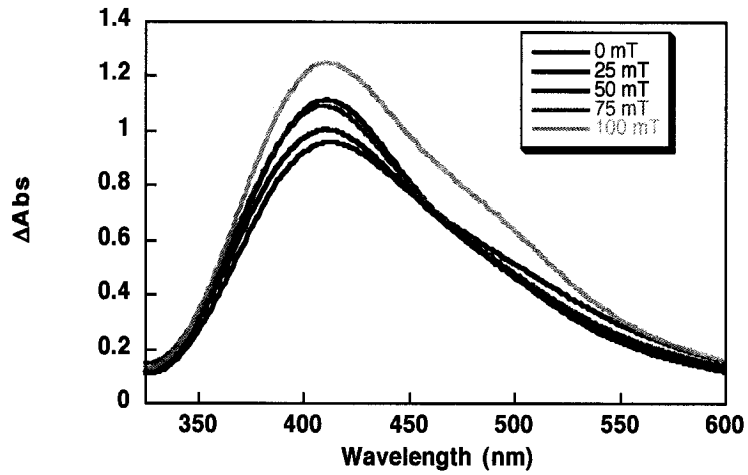

Figure 1.31: Plot of absorbance spectra of silver nanoparticles photogenerated in CTAN micelles in solutions of 0.025 M CTAN, 0.005 M BP. 0.01 M $AgNO_3$, and 0.04 M 1,4-CHD after vortex purging with nitrogen and 60 seconds of irradiation with an Oriel Xenon lamp and 320 nm cutoff filter. Pre-irradiation spectra have been subtracted.

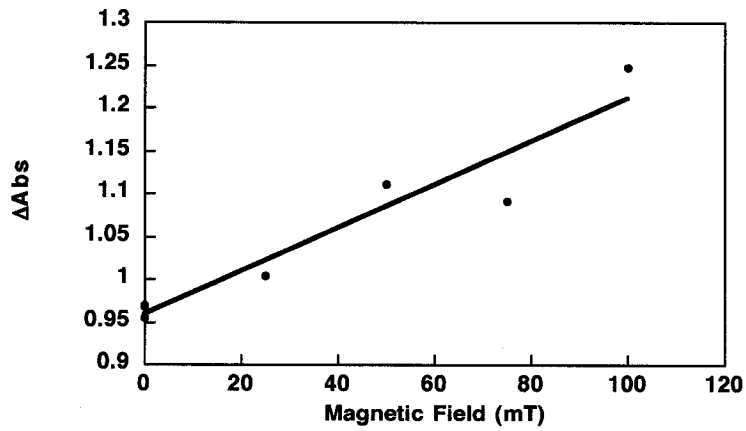

Figure 1.32: Plot of plasmon band intensity at 420 nm versus magnetic field strength for nanoparticles formed in CTAN. Experimental conditions are the same as Figure 1.31.

1.2.10. Studies on Ketyl Radicals Derived From Different Sources on the Generation of Silver Nanoparticles

The dependence of benzophenone on another molecule to act as a hydrogen donor hampers understanding of some of these processes and can facilitate Ag^+ quenching. Irgacure 2959 (Scheme 1.3) undergoes homolytic photocleavage to produce ketyl radicals, so the non-hydrogen-donating effects of molecules such as 1,4-CHD could be examined.

Scheme 1.3: Irgacure-2959 (2-hydroxy-1-[4-(2-hydroxyethoxy)phenyl]-2-methyl-1-propanone)

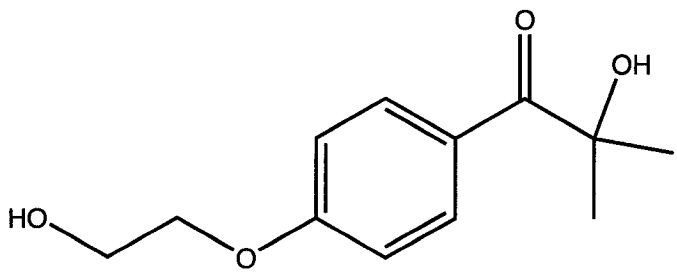

Irgacure forms silver nanoparticles faster than benzophenone. The plasmon band intensity following 15 seconds of irradiation of Irgacure in SDS micelles was comparable to that following 30 seconds of irradiation of benzophenone in the same system. Irgacure as the ketyl source in the absence of 1,4-CHD produces a reddish solution and the spectrum exhibits two overlapping peaks. The shoulder at about 525 nm has been attributed to aggregation (Figure 1.35). Replicate samples show slight variation, but when the spectra are plotted on the same graph, an isosbestic point becomes evident (Figure 1.33). These particles are very unstable, and precipitate as a black powder in the UV cell within 24 hours. Over the same time span, the λ_{max} of the spherical peak shifts from 425 nm to 433 nm. The spherical band decays rapidly for the first three hours after irradiation, decreasing from an absorbance of 1.3 to approximately 1 (Figure 1.36). Meanwhile, the aggregation band increases from 0.87 to a maximum of 1.05 at 15 minutes after irradiation before decreasing again. At 50 minutes after irradiation, both bands are approximately the same absorbance, and remain so for the remaining 12 hours of the experiment. At approximately 90 minutes after irradiation, the initial rapid decay of absorbance slows; over the next 3.5 hours, absorbance drops from ~0.9 to 0.73. After

this time, loss of absorbance increases and absorbance drops to 0.17 in 6 hours, with only minimal loss after this time. When 1,4-CHD is present, the 540 nm peak is not seen at all, and the absorbance of the 420 nm peak is significantly increased. If 1,4-CHD is added soon after irradiation, not only is this precipitation prevented, but the particles giving rise to the 420 nm peak are also selectively stabilised- the 525 nm peak vanishes and the 420 nm band increases (Figure 1.41).

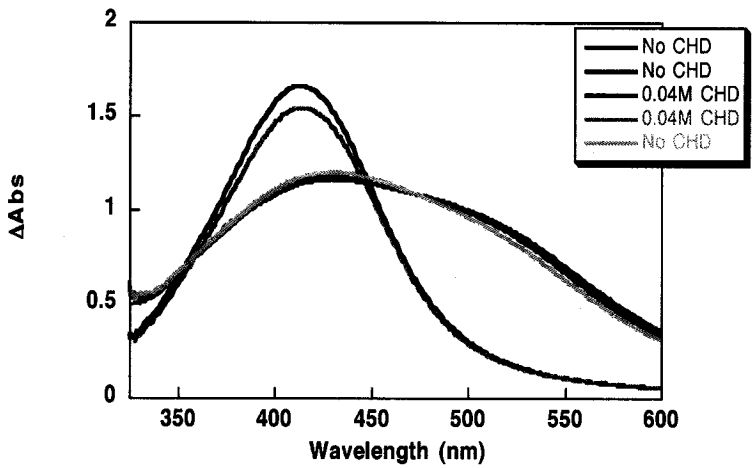

Figure 1.33: Absorbance spectra of replicate samples of silver nanoparticles photogenerated by ketyl radicals from Irgacure-2959 with and without 1,4-CHD. Solutions of 0.1 M SDS, 0.005 M Irgacure-2959 and 0.01 M $AgNO_3$ were vortex-purged and irradiation for 15 seconds with an Oriel Xenon lamp and 320 nm cutoff filter. Pre-irradiation spectra have been subtracted.

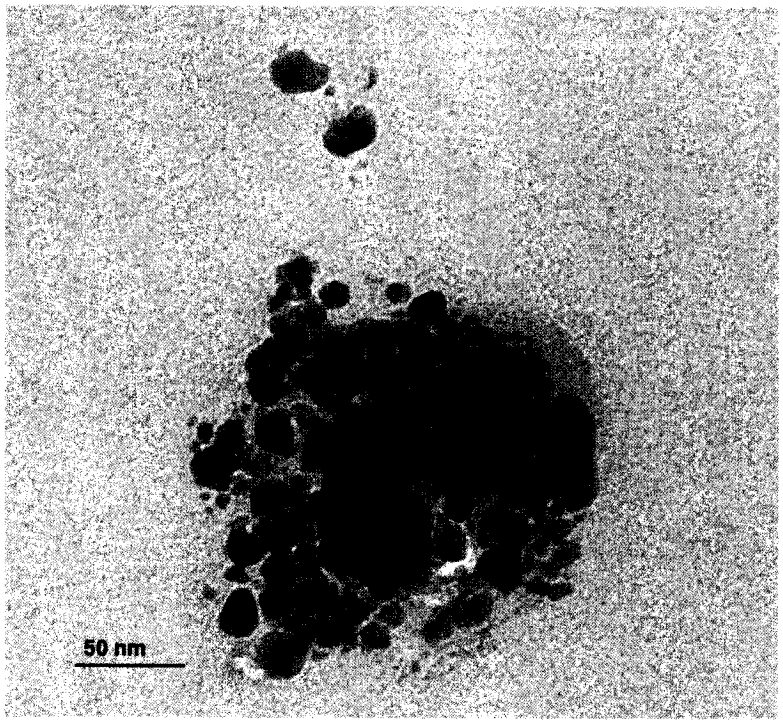

Figure 1.34: TEM images of silver nanoparticles photogenerated in an Irgacure-2959/SDS system without 1,4-CHD in the absence of a magnetic field from solutions of 0.1 M sodium dodecyl sulphate, 0.005 M Irgacure-2959 and 0.01 M $AgNO_3$ following vortex purging with nitrogen and 30 seconds irradiation with an Oriel Xenon lamp. 10 μL of solution was transferred by pipette to a 300 mesh carbon-coated copper TEM grid and then washed with MeOH. Image acquired at 200 kV.

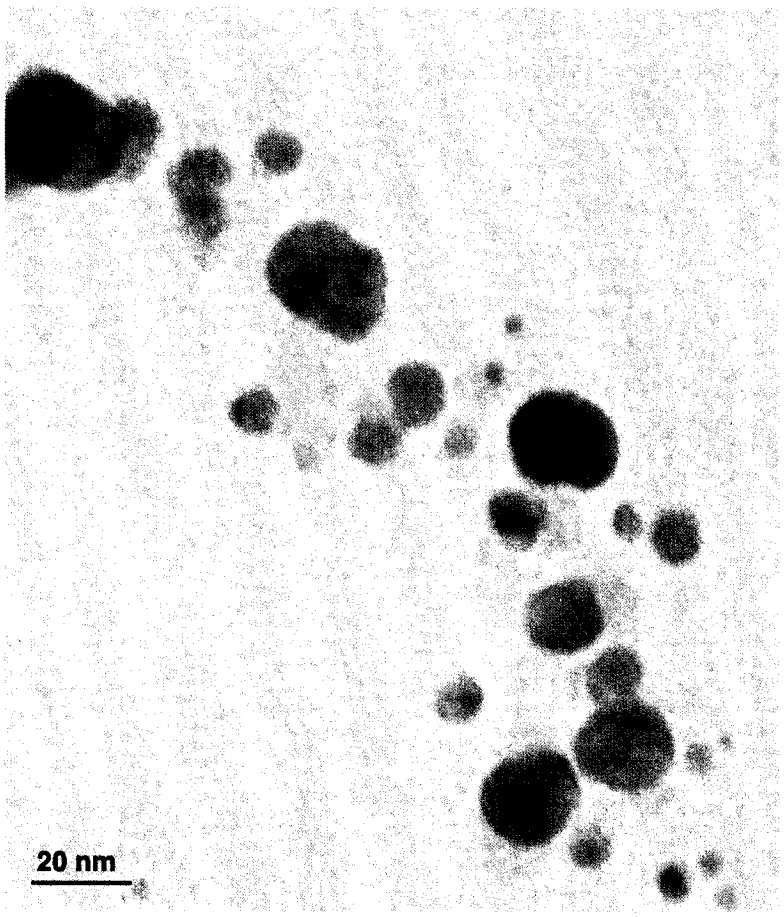

Figure 1.35: TEM images of silver nanoparticles photogenerated in an Irgacure-2959/SDS system with 1,4-CHD in the absence of a magnetic field from solutions of 0.1 M sodium dodecyl sulphate, 0.005 M Irgacure-2959, 0.04 M 1,4-cyclohexadiene and 0.01 M $AgNO_3$ following vortex purging with nitrogen and 30 seconds irradiation with an Oriel Xenon lamp. 10 μL of solution was transferred by pipette to a 300 mesh carbon-coated copper TEM grid and then washed with MeOH. Image acquired at 200 kV.

When irradiated in a magnetic field, samples without 1,4-CHD show no increase in absorbance over samples irradiated without a magnetic field (Figure 1.38). With 1,4-

CHD, a magnetic field effect is apparent between approximately 380-450 nm (Figure 1.39).

After 15 seconds of incremental irradiation, the absorbance of the plasmon bands for the Irgacure system is the same as that as the corresponding sample irradiated for 15 seconds continuously (Figure 1.40). The rate of nanoparticle formation is lower in the first 5 seconds than it is during the rest of the irradiation time.

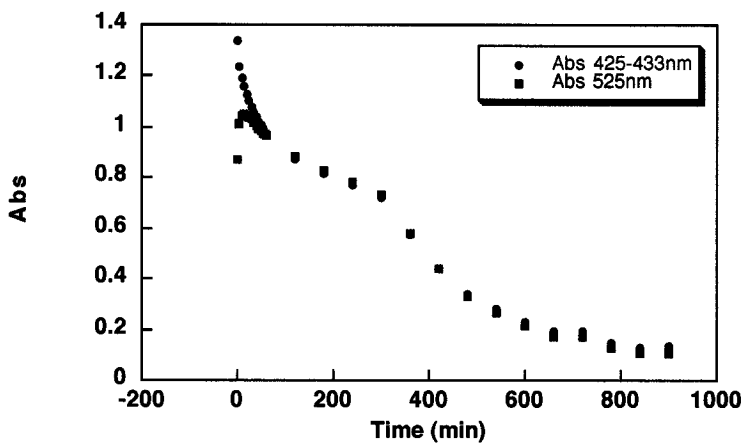

Figure 1.36: Plasmon band absorbance as a function of time after initial irradiation. Data points were collected every five minutes for one hour and then once every hour thereafter. Samples were kept in the dark between acquisitions. Nanoparticles were photogenerated by Irgacure-2959 from solutions of 0.1 M SDS, 0.005 M Irgacure-2959. 0.01 M $AgNO_3$ and 0 M 1,4-CHD after vortex purging with nitrogen and 15 seconds of irradiation with an Oriel Xenon lamp and 320 nm cutoff filter. Pre-irradiation spectra have not been subtracted.

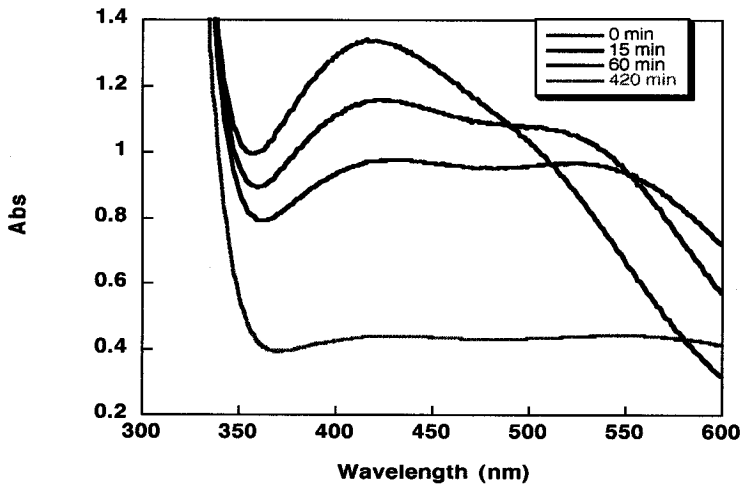

Figure 1.37: Selected spectra from which the data points in Figure 1.36 were derived, showing the evolution of spectral features over time. Experimental conditions are the same as for Figure 1.36.

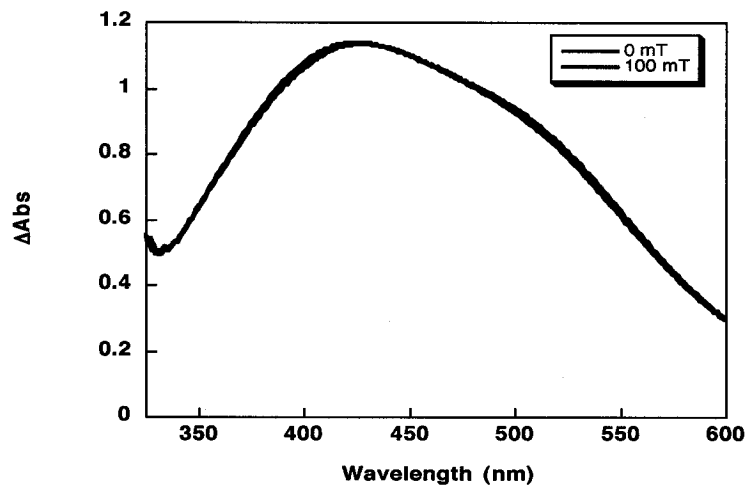

Figure 1.38: Absorbance spectra of silver nanoparticles photogenerated by ketyl radicals from Irgacure-2959, without 1,4-CHD, and with or without a magnetic field. Solutions of 0.1 M SDS, 0.005 M Irgacure-2959, 0.01 M $AgNO_3$ and 0 M 1,4-CHD were vortex-purged and irradiation for 15 seconds with an Oriel Xenon lamp and 320 nm cutoff filter. Pre-irradiation spectra have been subtracted.

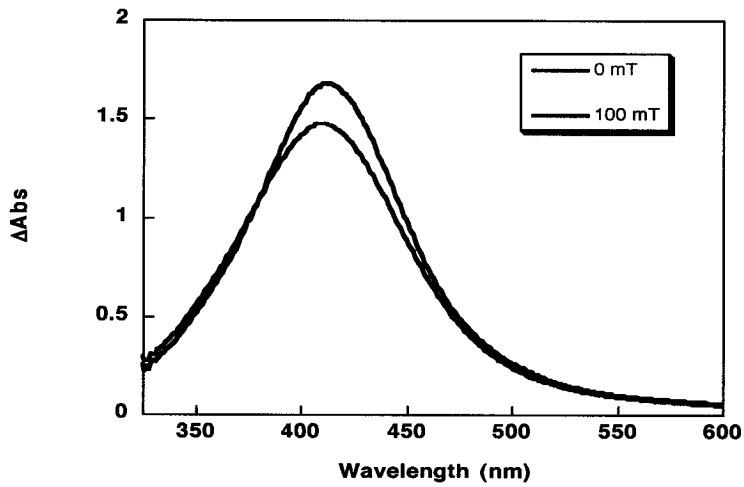

Figure 1.39: Absorbance spectra of silver nanoparticles photogenerated by ketyl radicals from Irgacure-2959, with 1,4-CHD, and with or without a magnetic field. Solutions of 0.1 M SDS, 0.005 M Irgacure-2959, 0.01 M $AgNO_3$ and 0 M 1,4-CHD were vortex-purged and irradiation for 15 seconds with an Oriel Xenon lamp and 320 nm cutoff filter. Pre-irradiation spectra have been subtracted.

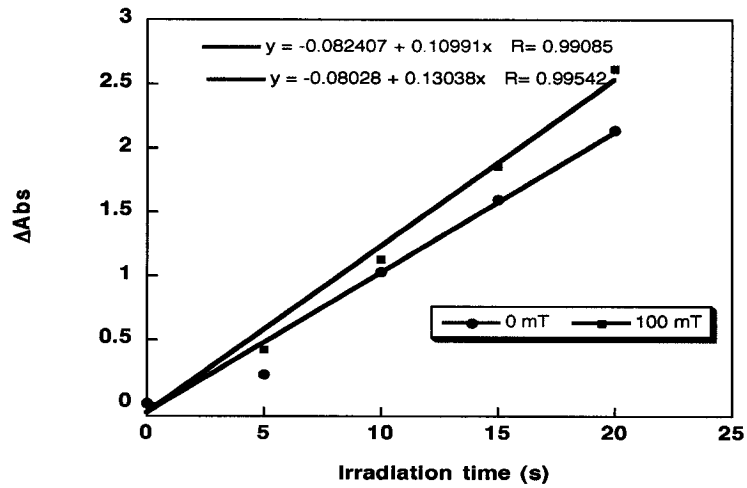

Figure 1.40: Plot of λ_{max} of plasmon bands of silver nanoparticles generated from ketyl radicals derived from Irgacure-2959 with respect to time in the presence and absence of a magnetic field in solutions of 0.1 M SDS, 0.005 M Irgacure-2959, 0.04 M 1,4-CHD and 0.01 M $AgNO_3$ after vortex purging with nitrogen and 20 seconds of irradiation in 5 second increments with an Oriel Xenon lamp and 320 nm cutoff filter. The pre-irradiation absorbance values have been subtracted from all data points.

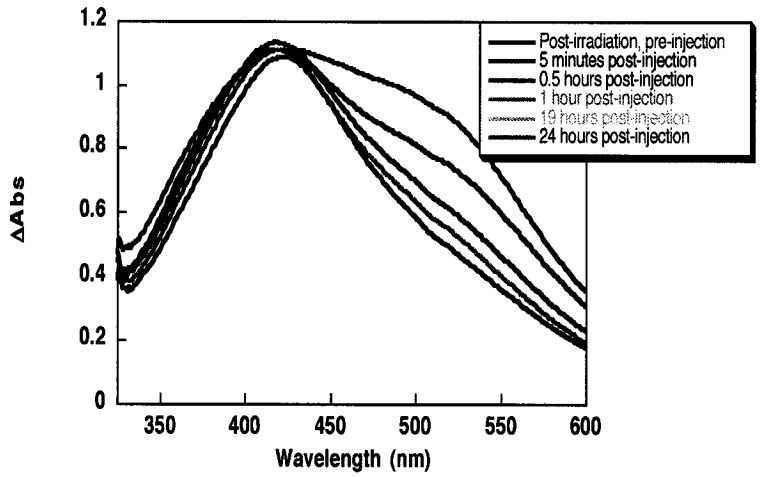

Figure 1.41: Absorbance spectra of silver nanoparticle plasmon bands with and without 0.04 M 1,4-CHD. Solutions of 0.1 M SDS, 0.005 M Irgacure-2959 and 0.01 M $AgNO_3$ were vortex-purged prior to irradiation. 0.04M 1,4-CHD was injected through the septa immediately after 15 seconds irradiation with an Oriel Xenon lamp and a 320 nm cutoff filter.

When photolysis is carried out using Irgacure-2959 and without SDS, the 540 nm band attributed to aggregation is favoured over the 420 nm discrete spherical particle peak, and is very broad (Figure 1.42). The absorbance of the 520 nm aggregated particle peak is approximately the same as that seen in the presence of SDS micelles, but the 420 nm spherical peak is greatly reduced.

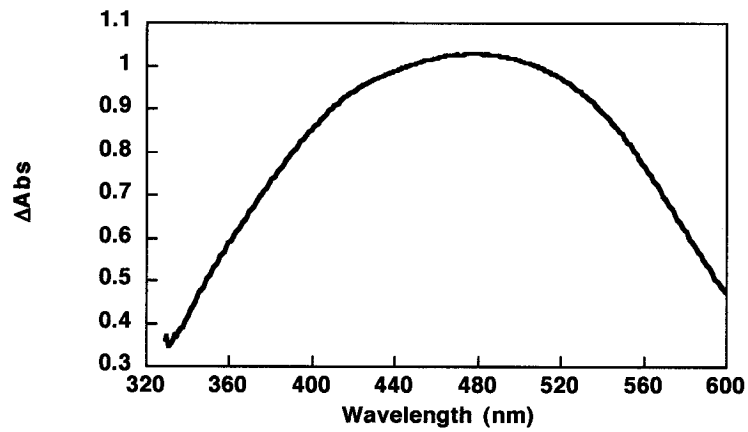

Figure 1.42: Absorbance of silver nanoparticles generated from Irgacure-derived ketyl radicals in a micelle-free solution containing 0.005 M Irgacure-2959, 0.01 M $AgNO_3$ after vortex purging with nitrogen and 15 seconds of irradiation with an Oriel Xenon lamp and 320 nm cutoff filter. The pre-irradiation spectrum has been subtracted.

When a sample of silver nanoparticles generated from Irgacure-2959 is injected with 1,4-CHD after irradiation and is then stored under nitrogen with a sealed septum (Figure 1.43), the band at 420 nm is stabilized in a similar manner to that seen when the sample is stored on the benchtop with a sealed septum (Figure 1.41). However, while absorbance of this band remains constant on the benchtop, it increases slightly when stored under nitrogen.

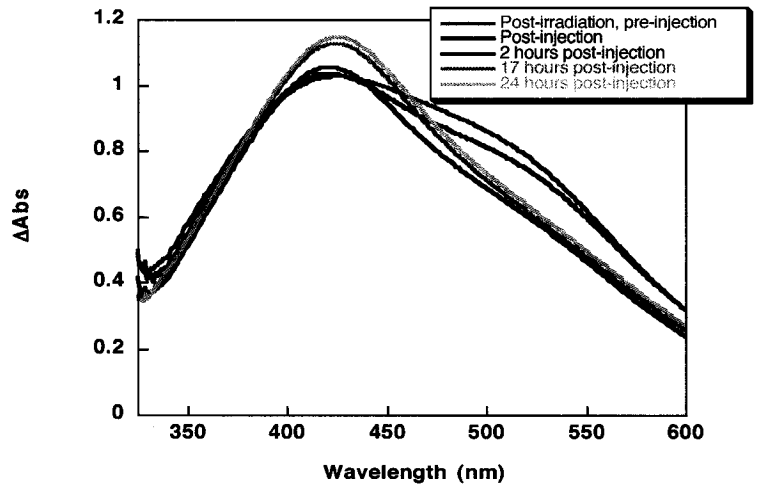

Figure 1.43: Absorbance spectra of silver nanoparticle plasmon bands before and after injection of 0.04 M 1,4-CHD. Solutions of 0.1 M SDS, 0.005 M Irgacure-2959 and 0.01 M $AgNO_3$ were vortex-purged prior to irradiation. 0.04 M 1,4-CHD was injected through the septa immediately after 15 seconds irradiation with an Oriel Xenon lamp and a 320 nm cutoff filter. The sample was subsequently stored under nitrogen in a glovebox.

1.2.11. Studies on the Effects of Exposure to Air on the Generation and Stability of Ag Nanoparticles

Solutions containing benzophenone and Irgacure-2959 that have not been purged with nitrogen do not efficiently generate nanoparticles. After 30 seconds of irradiation, an unpurged sample shows approximately 40% (0.44) of the plasmon absorption of a corresponding purged sample (1.16, Figure 1.44). After a further 30 seconds, the absorption is approximately two thirds (0.67) that of the purged sample. The plasmon band of the unpurged sample is also very broad, with the λ_{max} at longer wavelengths (432

nm at 30 seconds and 425 nm at 60 seconds for the unpurged sample, compared to 415 nm for the purged sample).

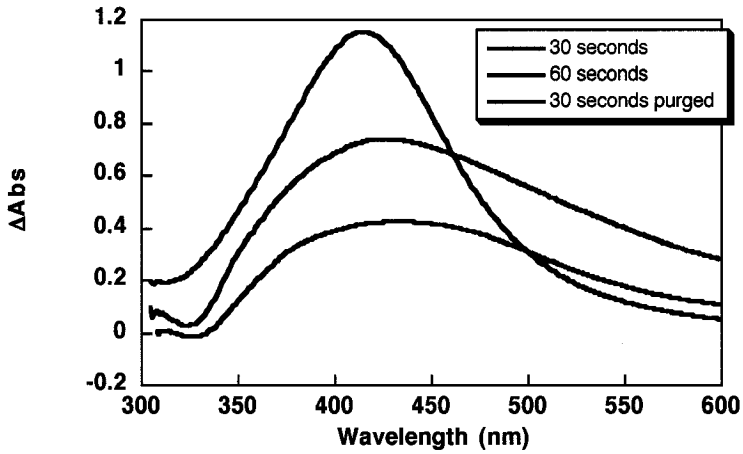

Figure 1.44: Absorbance spectra of silver nanoparticles photogenerated from purged and unpurged solutions of 0.1 M SDS, 0.005 M BP, 0.04 M 1,4-CHD and 0.01 M $AgNO_3$. Samples were irradiated for the times indicated with an Oriel Xenon lamp and 320 nm cutoff filter. All spectra have had the pre-irradiation absorbance subtracted.

When a solution containing nanoparticles was exposed to air in the dark, the particles remained unaggregated and continued to grow (Figure 1.45). There was little discernable difference between those formed in a magnetic field and those formed without it (Figure 1.46). After 1 hour of exposure to ambient atmosphere, the spectra of both samples are unchanged. After 1 day of exposure, the plasmon absorbance bands of both samples had increased slightly, with only minimal broadening of the peak. The samples were stored in the narrow-necked reaction cuvettes, which were wrapped in aluminium foil, and the cuvettes themselves were stored inside a metal box to minimize

exposure of the samples to light. As a result of being stored in the reaction cuvettes, the samples did not undergo any mechanical agitation as would be associated with transferring fluid between containers. Figure 1.47 shows the results of such agitation. After 1 hour, the plasmon band had broadened considerably, developing a shoulder at about 500 nm. In addition, the absorbance of the 420 nm peak decreased slightly. After 1 day, the plasmon band had decayed to almost nothing. The cause of this loss of absorbance was the black precipitate at the bottom of the UV cell.

Similar solutions left exposed to nitrogen in a glove box without mechanical agitation exhibited similar behaviour. After an hour, the spectra of samples photogenerated both with and without a magnetic field (Figures 1.48 and 1.49) had not changed substantially in either shape or absorbance, and after one day the plasmon absorbance bands have increased. A sample photogenerated without a magnetic field that was transferred between vessels to acquire the spectra showed no change after an hour and a large increase in absorbance across the entire spectrum after 1 day, a sign of substantial aggregation (Figure 1.50).

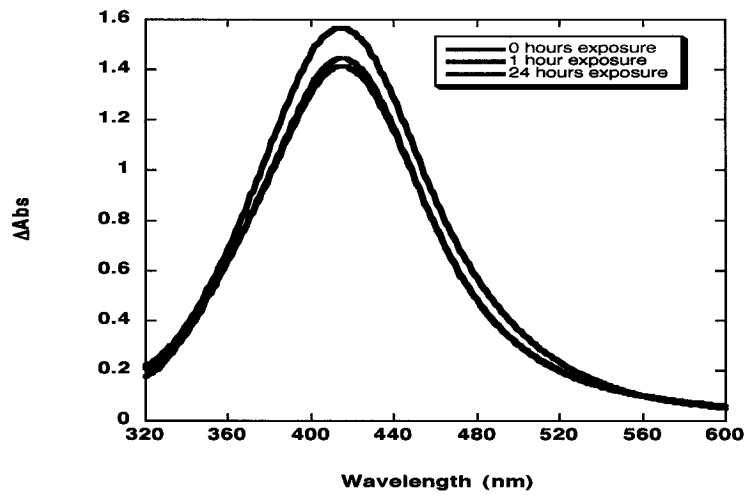

Figure 1.45: Absorbance spectra of silver nanoparticles photogenerated without a magnetic field from a solution of 0.1 M SDS, 0.005 M BP, 0.04 M 1,4-CHD and 0.01 M $AgNO_3$ after vortex purging with nitrogen and 30 seconds of irradiation with an Oriel Xenon lamp and 320 nm cutoff filter. Subsequent to irradiation, samples were exposed to air in the dark for the times indicated without mechanical agitation. All spectra have had the pre-irradiation absorbance subtracted.

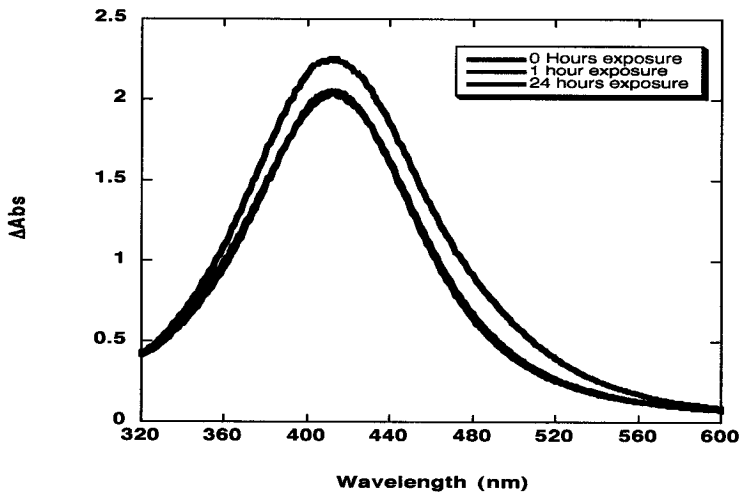

Figure 1.46: Absorbance spectra of silver nanoparticles photogenerated with a 100 mT magnetic field from a solution of 0.1 M SDS, 0.005 M BP, 0.04 M 1,4-CHD, 0.01 M $AgNO_3$ after vortex purging with nitrogen and 30 seconds of irradiation with an Oriel Xenon lamp and 320 nm cutoff filter. Subsequent to irradiation, samples were exposed to air in the dark for the times indicated without mechanical agitation. All spectra have had the pre-irradiation absorbance subtracted.

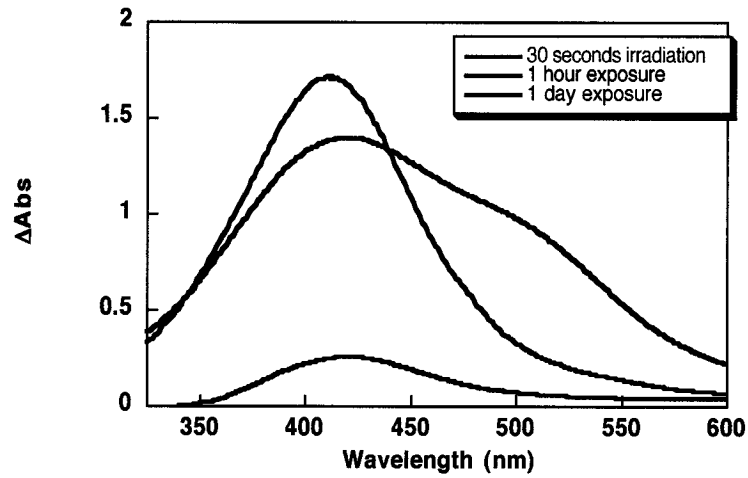

Figure 1.47: Absorbance spectra of silver nanoparticles photogenerated without a magnetic field from a solution of 0.1 M SDS, 0.005 M BP, 0.04 M 1,4-CHD and 0.01 M $AgNO_3$ after vortex purging with nitrogen and 30 seconds of irradiation with an Oriel Xenon lamp and 320 nm cutoff filter. Subsequent to irradiation, samples were exposed to air in the dark for the times indicated and underwent mechanical agitation during spectrum acquisition. All spectra have had the pre-irradiation absorbance subtracted.

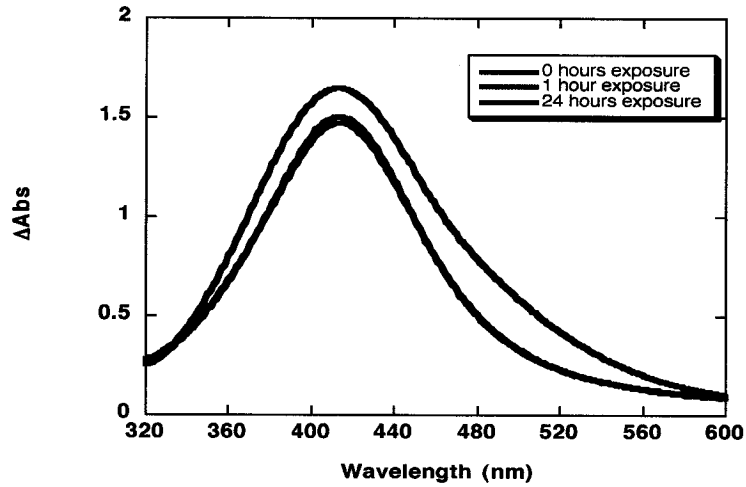

Figure 1.48: Absorbance spectra of silver nanoparticles photogenerated without a magnetic field from a solution of 0.1 M SDS, 0.005 M BP, 0.04 M 1,4-CHD, 0.01 M $AgNO_3$ after vortex purging with nitrogen and 30 seconds of irradiation with an Oriel Xenon lamp and 320 nm cutoff filter. Subsequent to irradiation, samples were uncapped in a nitrogen atmosphere glove box for the times indicated without mechanical agitation. All spectra have had the pre-irradiation absorbance subtracted.

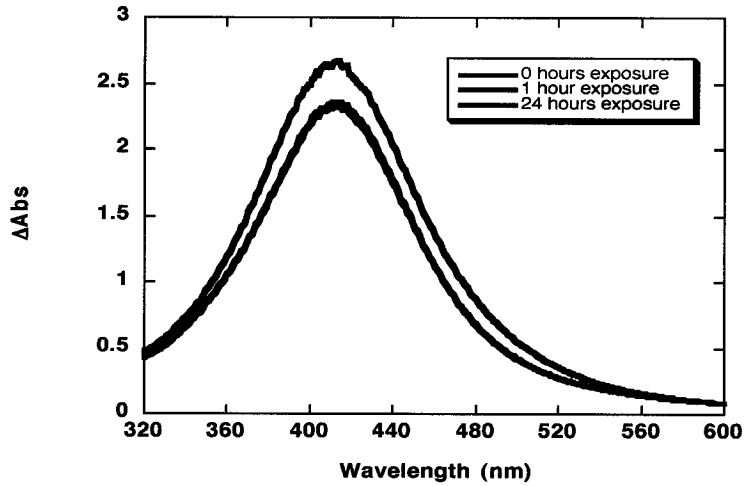

Figure 1.49: Absorbance spectra of silver nanoparticles photogenerated with a 100 mT magnetic field from a solution of 0.1 M SDS, 0.005 M BP, 0.04 M 1,4-CHD, 0.01 M $AgNO_3$ after vortex purging with nitrogen and 30 seconds of irradiation with an Oriel Xenon lamp and 320 nm cutoff filter. Subsequent to irradiation, samples were uncapped in a nitrogen atmosphere glove box for the times indicated without mechanical agitation. All spectra have had the pre-irradiation absorbance subtracted.

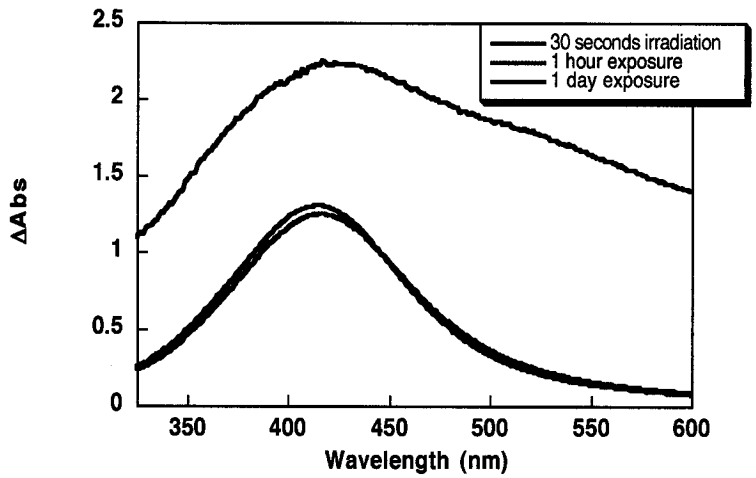

Figure 1.50: Absorbance spectra of silver nanoparticles photogenerated without a magnetic field from a solution of 0.1 M SDS, 0.005 M BP, 0.04 M 1,4-CHD, 0.01 M $AgNO_3$ after vortex purging with nitrogen and 30 seconds of irradiation with an Oriel Xenon lamp and 320 nm cutoff filter. Subsequent to irradiation, samples were uncapped in a nitrogen atmosphere glove box for the times indicated and underwent mechanical agitation during spectrum acquisition. All spectra have had the pre-irradiation absorbance subtracted.

1.2.12. Study on the Effects of other Dienes on the Formation and Stability of Silver Nanoparticles

In order to understand the role of alkenes on stabilising the nanoparticles, dienes less likely to donate hydrogen atoms to triplet benzophenone were selected. Photolysis of an SDS/BP/1,3-CHD system produced nanoparticles with a plasmon band possessing lower absorbance (~0.14) than that of a system with no 1,3-CHD (~0.16), with the peak wavelength was shifted to ~450 nm (Figure 1.51). When the experiment was repeated using Irgacure-2959 and 1,3-CHD, almost no nanoparticle generation occurred at all. A 100 mT magnetic field has no effect on this, the absorbance spectra of nanoparticles generated with and without the magnetic field being nearly superimposable (Figure 1.52).

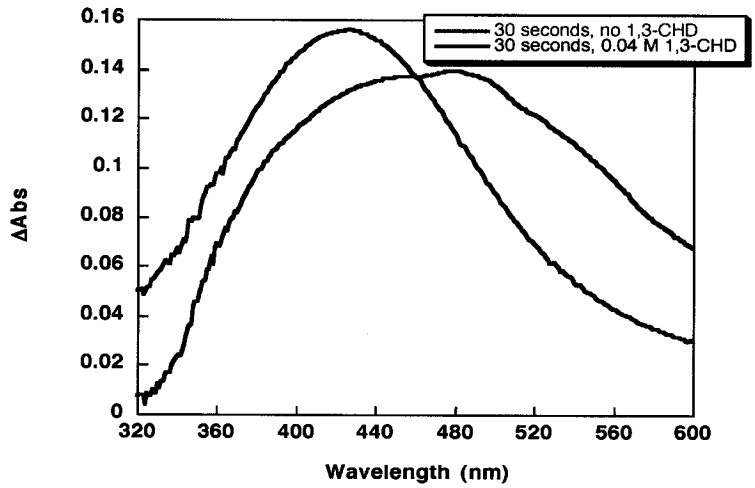

Figure 1.51: Absorbance spectra of silver nanoparticles generated from a solution of 0.1 M SDS, 0.005 M BP, 0.01 M $AgNO_3$, 0.04 M 1,3-CHD after vortex purging with nitrogen and 30 seconds of irradiation with an Oriel Xenon lamp and 320 nm cutoff filter. All spectra have had the pre-irradiation absorbance subtracted.

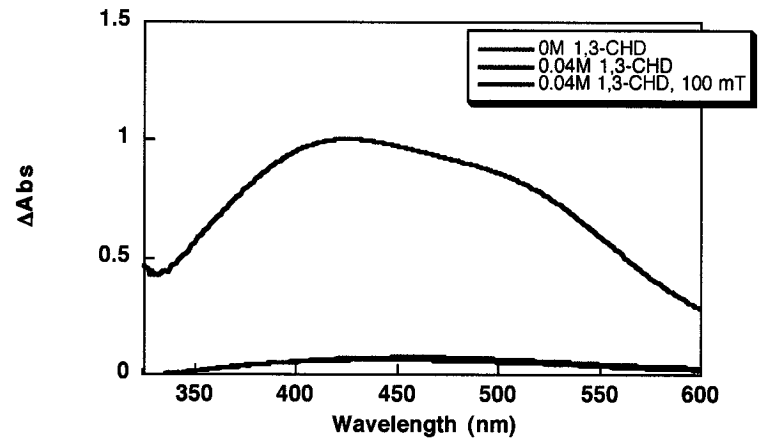

Figure 1.52: Absorbance spectra of silver nanoparticles generated from a solution of 0.1 M SDS, 0.005 M Irgacure-2959, 0.01 M $AgNO_3$ and 0.04 M 1,3-CHD after vortex purging with nitrogen and 30 seconds of irradiation with an Oriel Xenon lamp and 320 nm cutoff filter. All spectra have had the pre-irradiation absorbance subtracted.

In the SDS/BP system, stabilised spherical nanoparticles with an absorbance of about 0.25 are formed in the presence of 1,4-hexadiene (Figure 1.53). Aggregation is reduced in the presence of the diene, as can be seen in Figure 1.54.

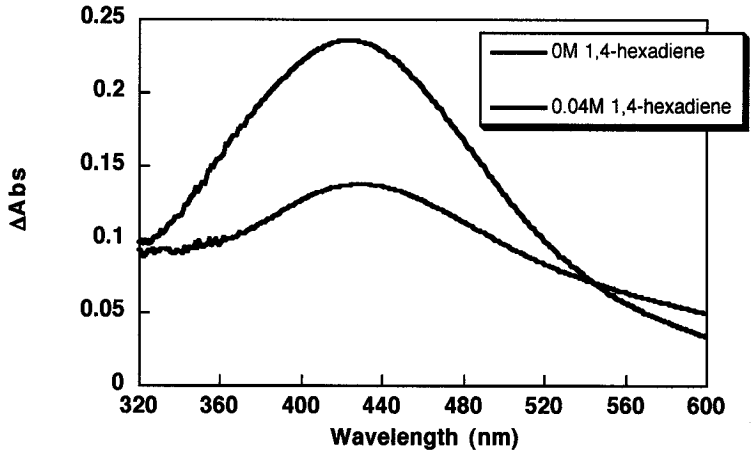

Figure 1.53: Effect of 1,4 hexadiene on nanoparticles generated from a solution of 0.1 M SDS, 0.005 M BP, 0.01 M $AgNO_3$ after vortex purging with nitrogen and 30 seconds irradiation with an Oriel Xenon lamp and 320 nm cutoff filter. All spectra have had the pre-irradiation absorbance subtracted.

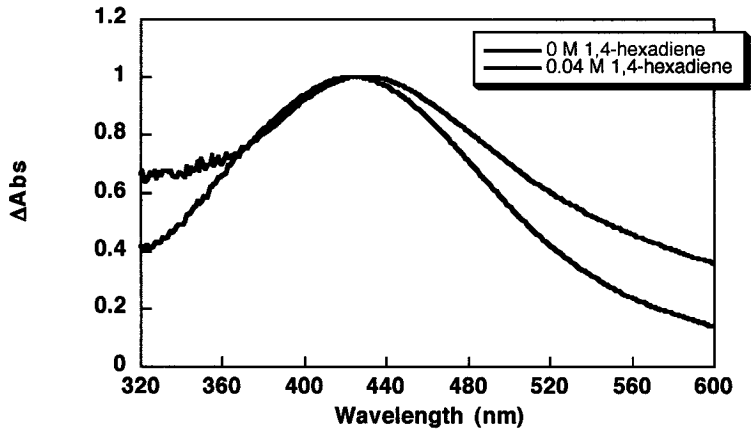

Figure 1.54: Absorbance spectra from Figure 1.53 normalised to λ_{max} to show effect of 1,4-hexadiene on peak width. Experimental conditions are the same as Figure 1.53.

1.3. Discussion

1.3.1. Introduction

The rate of photogeneration of silver nanoparticles from benzophenone ketyl radicals caged in micelles can be dramatically increased in an externally applied magnetic field. In the system outlined here, the efficiency of the reduction of silver(I) by ketyl radicals is governed by the rate at which the radicals exit the micelle. Once either half of the BPK-CHD radical pair exits, the geminate state is destroyed and recombination becomes an unlikely event. When triplet benzophenone reacts with the surfactant, the exit rate constant for the ketyl radical is about 7% of the overall radical pair decay rate; very few ketyl radicals exit the micelle before recombination occurs, even in the presence of a magnetic field that causes Zeeman splitting of the triplet sublevels.[85] The exit rate for the SDS-derived radical is on the same order as the rate of exchange of surfactant molecules between the solution and micelle cage, occurring on the order of microseconds[87] and is small on the time scale under consideration. The radical derived from 1,4-CHD - added as a hydrogen donor - exits much faster (4.4×10^6 s^{-1}),[85] which destroys the geminate state and effectively increases the escape efficiency of the ketyl radical and hence the reduction of Ag^+. Since the 1,4-CHD radical has departed, recombination with the ketyl radical cannot occur.[85]

As the magnetic field increases, the T_+ and T_- sublevels move farther apart energetically from the barycentre and from the singlet state, slowing the rate of radical-pair intersystem crossing and thus of geminate radical recombination. Once a certain

field strength is reached, the difference in energy levels is so great that recombination from the T_+ and T_- sublevels can be shut off completely. Beyond this point, no further enhancement of the lifetime of the ketyl radical is possible, and the lifetime is limited by the escape efficiency and by recombination from the T_0 sublevel, which has not moved energetically. This is seen in the experimental results (Figure 1.21). The absorbance at the plateau reached at 750 mT represents an approximate 67% increase over the absorbance at 0 mT. This is consistent with a 2/3 increase in the availability of separated ketyl radicals resulting from fewer in-cage recombinations due to Zeeman splitting of the triplet sublevels.

TEM imaging (Figure 1.27) indicates that these particles are roughly spherical and polycrystalline – that is, the orientation of the crystal lattice varies from domain to domain within a single nanoparticle. This is the result of several centres of nucleation clustering together and growing into a stable particle.

1.3.2. Reactive Intermediate Formation in Nanoparticle Photogeneration

1.3.2.1. Triplet Benzophenone Quenching by Ag^+

Ag^+ quenches the triplet state of benzophenone quite readily, which means that the silver ions compete with the hydrogen atom donor for triplet quenching. If the quenching by silver is too efficient, the process of nanoparticle formation can be

impeded. The rate of this quenching was determined by laser flash photolysis. The n-π^* transition of benzophenone absorbs at 350 nm, thus a 355 nm laser was chosen as the excitation source. The decay of the triplet was monitored at 530 nm. The quenching rate constant of 5.8 x 10^9 M^{-1} s^{-1}, obtained from a plot of the pseudo-first order triplet decay rate constant as a function of [Ag^+], is close to diffusion control in water. This quenching is dynamic rather than static in nature, as indicated by the fact that there is no initial decrease in the triplet absorbance immediately after the laser pulse. In other words, the triplet and the silver cation have to "find" each other through diffusion, rather than occupying a pre-existing sphere of quenching where the quencher can act upon the triplet immediately after it is formed. This strongly suggests that silver cations do not enter the micelles, and that the quenching spheres of the ions do not extend into the interior of the micelles. Electron exchange processes require close proximity.

The effect of the magnetic field on the rate of micellar escape of the BPK-1,4-CHD geminate radical pair in the absence of silver can be seen from the transient decay traces monitored at 530 nm (Figures 1.3 and 1.4). The benzophenone ketyl radical is responsible for the long-lived signal (hundreds of nanoseconds) after the initial decay because the 1,4-CHD radical escaped the radical pair and then the micelle cage rather than recombining and forming geminate products. This signal still decays slowly, since radicals are by their very nature unstable species, but this decay is trivial on the timescale under consideration. In the absence of a magnetic field, a very small percentage (~12%) of these radicals survives for more than 100 ns.

Laser flash photolysis was also employed in an attempt to monitor the kinetics of the growth of the plasmon band at 420 nm in real time. This failed due to the 1 ms window of the instrument being too short to observe growth at nucleation sites. It is safe therefore to say that, based on this result and the results of the time-resolved experiment (Figure 1.22) in which a plasmon band is visible after five seconds of irradiation, nucleation and growth of the particles occurs between the millisecond and second time domains.

1.3.2.2. Hydrogen-donor: 1,4-Cyclohexadiene

The most dramatic and unusual effects in this study are associated with 1,4-CHD. First and foremost, the compound is a very good hydrogen donor as the resultant cyclohexadienyl radical is stabilised by the formation of a delocalised π-system across five of the six carbons in the ring (Scheme 1.2). In the absence of 1,4-CHD, triplet benzophenone reacts with the C-H bonds in the aliphatic tail of the SDS molecules of the micelle cage. This process is less efficient due to the instability of the resulting secondary carbon-centred radicals compared to the 1,4-CHD radical, hence the lower nanoparticle yield. In addition, the 1,4-CHD-derived radical readily escapes from the micellar cage, thereby destroying the geminate state and increasing the lifetime of the corresponding ketyl radical, while the SDS-derived radical does not.

The plasmon band is very broad and unsymmetrical without 1,4-CHD, indicating that the particles are forming aggregates.[88] When 1,4-CHD is present, the plasmon

band is observed to be narrower, corresponding to a lower degree of aggregation. This phenomenon is depends on concentration; the width of the absorbance band varies inversely with the concentration of 1,4-CHD. Alkenes are known to adsorb onto noble metal surfaces; surface-enhanced Raman scattering is based upon this principle.[89] Clearly, the 1,4-CHD is adsorbing onto the particles, stabilising them and preventing their aggregation. Pre-existing aggregation can be reversed as well: 1,4-CHD injected into a UV cell containing nanoparticles that have been photogenerated without it causes the solution to become less brown and more golden-yellow, indicating that many of the larger aggregates are being broken up. This conclusion is supported by the spectra; five hours after injection (Figure 1.15), the absorbance stemming from aggregation was greatly reduced compared to the pre-injection spectrum and the λ_{max} had shifted to shorter wavelengths. The aggregation in the 1,4-CHD-free control sample increased quite noticeably, as indicated by the growth of the tail into a shoulder. Seventy-two hours after injection (Figure 1.14), the 1,4-CHD-added plasmon band was slightly narrower (fwhm) than the 5 hour spectrum, while the spectrum of the sample without 1,4-CHD had broadened considerably. In addition, the recovery of the absorbance after 72 hours stored in the dark suggests that the particles continue to grow by non-photochemical means, probably by Ostwald ripening.[70] It is difficult to determine the presence of Ostwald ripening in the spectra of the sample containing 1,4-CHD since the aggregation effects are much more dramatic. However, the absorbance of the surface decreases and narrows between 350 and 400 nm, the region of the spectrum corresponding to the smallest nanocrystals. Therefore, while growth as a result of Ostwald ripening is probably arrested by the 1,4-CHD, the dissolution of the unstable

small particles is not. Clearly, 1,4-CHD acts as a stabilising ligand in this system, preventing aggregation and breaking up aggregates after they have formed.

While normally insoluble in water, 1,4-CHD forms water-soluble adducts with Ag^+. Using a K_{eq} of 4.9 given by Muhs and Weiss[90] for the reaction

$$Ag^+ + CHD \leftrightarrows AgCHD^+ \qquad \text{Equation 1.1}$$

the concentration of the silver-diene complex is calculated to be 1.96 mM from the equilibrium expression

$$K_{eq} = \frac{[Ag(CHD)^+]}{[Ag^+][CHD]} \qquad \text{Equation 1.2}$$

under experimental conditions of 10 mM Ag^+ and 40 mM CHD. Therefore, the vast majority of the 1,4-CHD resides in the micelles where it can easily react with the benzophenone triplet, but enough is associated with the silver cation to stabilise nascent nanoparticles as they grow.

Table 1.1 Effects of [CHD] on the plasmon absorbance and formation of silver-olefin complex

[1,4-CHD] (mM)	1,4-CHD:Ag^+	$[Ag(1,4\text{-CHD})^+]$[1] (mM)	λ_{max}	Peak ΔOD	Peak width (fwhm) (nm)
10	1	0.49	417	.96	120
20	2	0.98	415	1.4	110
30	3	1.47	412	1.4	104
40	4	1.96	412	2.0	94

[1] – determined from Equation 1.2

As the concentration of 1,4-CHD increases, there is a trend toward shorter wavelengths and narrower peak widths of the plasmon band, indicating smaller, more monodisperse, less aggregated particles. Peak width decreases linearly with increasing concentration across the entire range of [1,4-CHD] examined (Table 1.1). As peak width is a measure of aggregation, this indicates that higher concentrations of 1,4-CHD result in less aggregation. The λ_{max} of the plasmon band also decreases slightly from 10 mM to 30 mM. This is a result of the capping effect[91] of the 1,4-CHD: as the nanoparticle is formed, alkene molecules adsorb onto its surface, stopping its growth and resulting in plasmon bands with a peak absorbance at shorter wavelengths. At higher concentrations of alkene, this adsorption takes place faster, which stops the growth of the particles earlier, resulting in smaller nanocrystals.

The intensity of the peak, however, more than doubles between 10 mM and 40 mM 1,4-CHD, which indicates an increased number of smaller particles. This reflects the role that the diene plays in accelerating the rate of nanoparticle formation through hydrogen donation to the benzophenone triplet to form ketyl radicals.

In addition, the increase in 1,4-CHD concentration means that the diene will out compete the Ag^+ cations for benzophenone triplets, resulting in a higher yield of ketyl radicals.

1.3.2.3. Nature of the Interaction Between 1,4-Cyclohexadiene and Silver Nanoparticles

The bond between the adsorbed 1,4-CHD and the nanoparticles is not very strong. The adduct does not show any additional absorbance band in the UV or visible spectra assignable to charge transfer or similar phenomena, and the IR spectrum was impossible to obtain on salt plates because all of the 1,4-CHD evaporated. 1,4-Cyclohexadiene has distinctive peaks at 3029 cm^{-1}, 2882 cm^{-1}, 1642 cm^{-1}, 1430 cm^{-1}, 964 cm^{-1} and 625cm^{-1},[92] and none of these were present in the IR spectrum of the sample prepared from acetonitrile. 1,4-Cyclohexadiene is very volatile (BP 81-82 °C) and evaporates very readily at room temperature. In addition, extraction into organic solvents removed the BP, SDS and 1,4-CHD but failed to transfer any nanoparticles. Instead, removal of the stabilising adsorbed organic species caused instant aggregation. This combined with basic Surface-Enhanced Raman Scattering (SERS) theory[93] strongly suggests that the organic molecules are adsorbed on the surface of the particle and not chemically bonded. This contradicts the literature,[88] which states that replacing a charged adsorbate with an uncharged molecule - in this case, 1,4-CHD - will enhance

aggregation, not prevent it. This is clearly not the case in this instance, which suggests that the SDS surfactant molecules are not being displaced. Instead, the 1,4-CHD molecules are located within the hydrophobic region of the surfactant layer immediately adjacent to the nanoparticle surface (Scheme 1.4)

Scheme 1.4: Schematic depiction of the arrangement of surfactant and diene molecules on nanoparticle surface

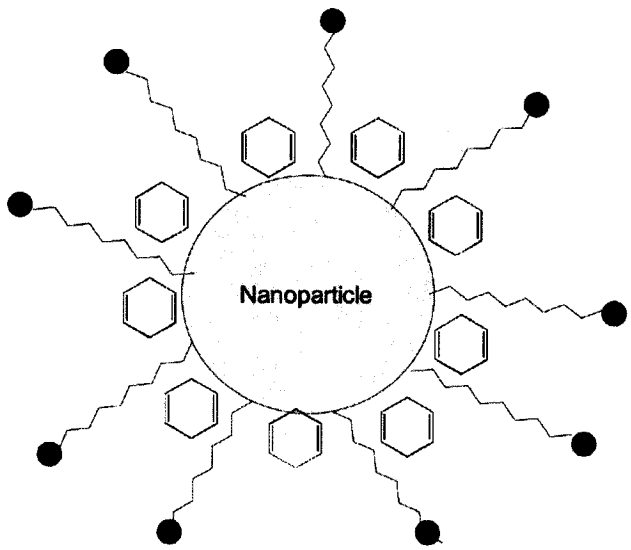

1.3.2.4. Benzhydrol as a Source of Hydrogen Atoms and Ketyl Radicals

When benzophenone abstracts a hydrogen atom from benzhydrol, two identical ketyl radicals are formed (Scheme 1.5).[94] The process is slower than the abstraction from 1,4-CHD, but it was hoped that the potential doubling in yield might make up for

this slower reaction. Both halves of this pair are equally likely to exit the micelle. If the exit rate of the SDS-derived radical is assumed to be negligible (a reasonable assumption, since the rate of escape will be the same as the rate of exchange between the micelle cage and free surfactants, which is very long compared to the species under consideration here),[87] the escape efficiency of the BPK-BPK radical pair should be approximately twice the BPK-SDS radical pair. This is seen in the results, as after 60 seconds of irradiation the absorbance of the plasmon band produced from the benzhydrol/benzophenone system is approximately double (~0.4, Figure 1.29) that seen for the BPK-SDS radical pair after the same irradiation time (~0.2, Figure 1.13). However, the plasmon band is much smaller than that produced from a system containing 1,4-CHD, which typically exceeds an absorption of 1.0 after half the irradiation time of the benzhydrol system.

At 100 mT, only a 45% increase in the absorbance of the plasmon band is seen, and no plateau region comparable to that seen in the SDS/BP/1,4-CHD system is evident. This suggests that the triplet and singlet states of the BPK-BPK radical pair are closer in energy than BPK-1,4-CHD and require a stronger magnetic field to split them sufficiently to shut off recombination from the T_+ and T_- sublevels. As our experimental setup was only able to reach 120 mT, this could not be investigated.

However, with no alkene present to stabilise the particles, aggregation was substantial, more so at higher field intensities. 1,4-Cyclohexadiene was not added, since it would vastly out-compete benzhydrol in reacting with the benzophenone triplet.

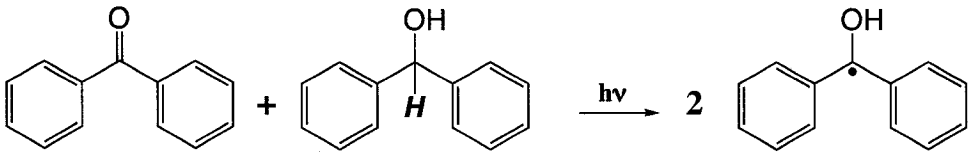

Scheme 1.5: Photogeneration of ketyl radicals from benzophenone and benzhydrol

1.3.2.5. Studies of Ketyl Radicals Derived From Different Sources on the Generation of Silver Nanoparticles

Irgacure-2959 is a water-soluble photoinitiator from CIBA Specialty Chemicals marketed as a product for the curing of paints, although it can also be used as an initiator in the photopolymerisation of liquid crystals.[95] Upon irradiation, it undergoes very rapid homolytic cleavage (Norrish Type I) to produce a benzoyl radical and an acetone-derived ketyl radical (Scheme 1.6).

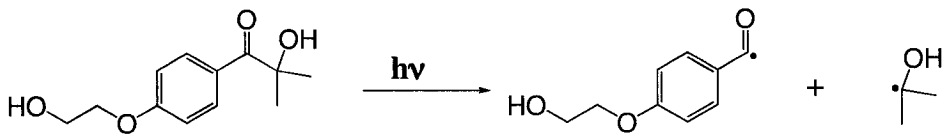

Scheme 1.6: Photodissociation of Irgacure-2959

Because this reaction depends only on the unimolecular absorption of a photon, the rate of photogeneration of nanoparticles is much faster than the formation of particles from benzophenone-derived ketyl radicals, which must abstract a hydrogen atom from another molecule before reducing the silver ions; as a result, the triplet state of the Irgacure molecule is much shorter lived than the benzophenone triplet, and there is much

less opportunity for silver ions to quench this triplet. In addition, the Irgacure molecule is water-soluble and does not require the presence of micelles, so there is no rate-limiting escape process. However, this also removes, the cage effect required for magnetic field effects. The presence of 1,4-CHD makes no difference to the rate of formation, but it does appear to have a stabilising effect on the nanoparticles formed. With 1,4-CHD present, the usual spherical nanoparticles form and are stable for long periods of time, on the order of a few (~3) days. Without it, two distinct bands are formed, attributed to the discrete spherical particles and aggregates of those nanoparticles visible in TEM images.[88] These aggregates are very unstable, aggregating further and precipitating within approximately 13 hours. The septa used to seal the UV cuvettes do not reliably exclude oxygen over this timespan, and it is likely that some oxygen was injected into the cuvette along with the CHD after purging was complete. It is likely that this oxygen contamination could cause the particles to oxidise.[96] However, this process occurs even when the cuvettes are stored under nitrogen in a glovebox, albeit much slower (between 24 and 40 hours), so while the aggregation and precipitation of the particles is not caused solely by the presence of oxygen, the rate of aggregation is enhanced by it.

When 1,4-CHD is injected into sealed cuvettes containing nanoparticles generated from Irgacure without CHD, effects resembling those observed under similar conditions in the BP/SDS system are noted. After 24 hours, no major loss of intensity of the plasmon band is noted (Figure 1.41), as compared to the total precipitation after 13 hours of samples containing no 1,4-CHD. In addition, the aggregation band around 500 nm decreases with time, eventually becoming a slight shoulder after 24 hours. This

phenomenon is seen in the literature on a longer timescale. Nanoparticles prepared by Egorova and Revina[96] through radiochemical synthesis show a broad spectrum 40 minutes after irradiation, with a peak at around 520 nm. Reverse-phase micelles of AOT (sodium bis-(2-ethylhexyl)sulfosuccinate in isooctane are employed in this preparation, and the synthesis takes place in the solubilised water pools of these micelles. These conditions do not stabilise the particles in the same manner as normal-phase micelles: the resulting spectrum looks similar to the one of nanoparticles synthesised without micelles shown in Figure 1.42, although with a much lower absorbance. Two weeks after synthesis, the typical spherical plasmon band at ~400 nm emerges. No explanation for these changes is offered by these authors, but in light of the results presented here, it seems likely that the aggregates of particles separated over time.

1.3.2.6. Effects of Other Dienes as Particle Stabilisers

In order to test the effects of alkenes on the growth and stabilization of particles, 1,3-cyclohexadiene (1,3-CHD) was used instead of 1,4-CHD. 1,3-Cyclohexadiene is a very good hydrogen donor similar to but less efficient than 1,4-CHD due to the lack of a resonance-stabilised radical form. However, due to its conjugated π-system, it is also an excellent triplet quencher. Because of this, the benzophenone triplet decays by energy transfer under these conditions rather than the formation of ketyl radicals, resulting in plasmon bands vastly reduced compared to those generated with 1,4-CHD. Even under these conditions, though, some nanoparticle production does occur (Figure 1.51). The irregularities seen in the spectrum are attributed to the presence of polymerised 1,3-

CHD. To get around this problem, the experiment was repeated using Irgacure-2959, which does not require a hydrogen donor to react with a triplet state in order to produce ketyl radicals. Unfortunately, the production of ketyl radicals was quenched completely under these conditions (Figure 1.52), suggesting that the Irgacure molecule exists in an excited triplet state just before dissociation into a radical pair.

1,4-hexadiene (1,4-HD) is a less-efficient triplet quencher and hydrogen donor compared to the 1,4-CHD. The lack of resonance arising from its linear structure means that the radical resulting from H-abstraction is less stabilised compared with the doubly allylic system in 1,4-CHD. Despite this, 1.4-HD is still an effective H-donor in its own right, and the lack of nanoparticle formation is most likely due to Ag^+ quenching of the benzophenone triplet. In the SDS/BP system, stabilised spherical nanoparticles with an absorbance of about 0.25 are formed (Figure 1.53). The plasmon band is narrowed and blue shifted slightly compared to a sample without any diene. The lack of a good hydrogen donor sharply reduced the rate of photogeneration, but the presence of an alkene stabilises the particles that do form.

1.3.3. Effects of Micelles on the Photogeneration and Stability of Silver Nanoparticles

In addition to solubilising the benzophenone in aqueous solution, the SDS micelles provide a cage in which the geminate radical pair can undergo radical reactions that can be influenced by Zeeman splitting of the triplet sublevels.

1.3.3.1. Cationic micelles

The most common cationic surfactants are cetyltrimethylammonium chloride (CTAC) and bromide (CTAB); both are commercially available and reasonably inexpensive. However, halide ions react rapidly with Ag^+, leading to precipitates, with solubility products of 1.76 x 10^{-10} M^2 for AgCl and 5.35 x 10^{-13} M^2 for AgBr.[97] Cetyltrimethylammonium nitrate (CTAN) will solubilise benzophenone and cage the geminate radical pair without precipitating Ag^+ and can be prepared easily from CTAB by treating it with $AgNO_3$.[98] Magnetic field effects were seen with this system on a comparable scale to SDS micelles. When solutions of CTAN were prepared at a concentration close to that used for the SDS system, they were found to be quite viscous, which made mixing with a vortex mixer less effective and resulted in rates of diffusion that differed from the SDS system, rendering invalid comparisons between the two systems. As a result, much lower concentrations were employed in the case of CTAN. Because the critical micelle concentrations of CTAN is so much lower than that of SDS (5.79 x 10^5 M[99] compared to 0.0082 M[87]), it was not possible to achieve similar conditions at identical concentration of surfactant.

When the portions of the spectra not overlapped by the secondary aggregation shoulder are considered, the shape of the plasmon band does not appear to be radically different from that shown by nanoparticles generated from the BP/SDS system. This suggests that the aliphatic chains of the micelles behave similarly to stabilise the

spherical particles, and the stabilisation is not affected by the charge sign of the head group.

Despite the greater escape efficiency of ketyl radicals from cetyltrimethyl-based micelles compared to SDS micelles,[85] the yield of nanoparticles as monitored by the 420 nm plasmon band is about 67% of that seen in SDS after twice the irradiation time. The band also has a shoulder at around 500 nm, indicative of aggregation.[88] This is an unexpected result, given the presence of 1,4-CHD and its stabilising effects in the BP/SDS system. However, the concentration of surfactant in this case is approximately one quarter that of the SDS system, resulting in a much lower surfactant:Ag^+ ratio and hence less stabilisation. Irradiation carried out at 100 mM CTAN produced a much cleaner yellow colour, although air bubbles associated with the high viscosity of this solution made acquisition of interference-free spectra impossible. This suggests that both the surfactant and 1,4-CHD play a role, possibly cooperative, in reducing the aggregation of silver nanoparticles.

Another factor that must be considered is the sign of the charge on the headgroup of the surfactant molecule. An anionic micelle will have a Gouy-Chapman electrical double-layer of cations surrounding it,[87] consisting of Na^+ and Ag^+ associating with the sulphate headgroups in the SDS/BP system (Scheme 1.7). A cationic CTAN micelle, on the other hand, will have a layer of nitrate anions surrounding the quaternary ammonium headgroup. A ketyl radical exiting an SDS micelle, therefore, will be much more likely to encounter an Ag^+ cation almost immediately than the same radical exiting a CTAN

micelle. In addition, Ag^+ will be repelled by free quaternary ammonium surfactants and attracted to sulphate surfactants, which means that a stabilising layer will be immediately available upon formation of nucleation centres.

Scheme 1.7: Gouy-Chapman layers surrounding SDS (left) and CTAN (right) micelles

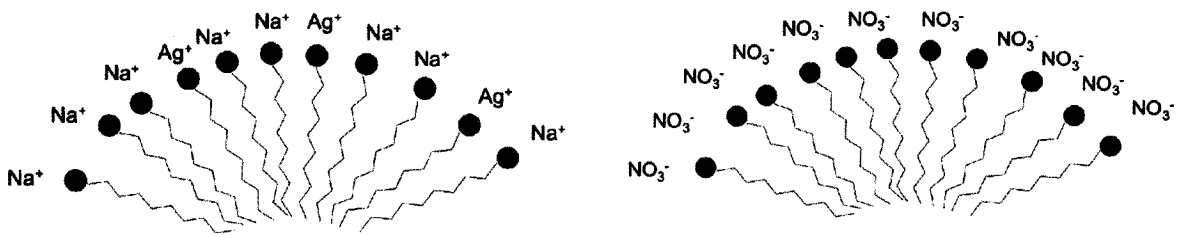

Sodium dodecyl sulphate Cetyltrimethylammonium nitrate

The magnetic field effects on the spherical nanoparticle peak formed in CTAN are not as pronounced as for SDS (32% increase in absorption at 100 mT for CTAN compared to 67% for SDS), which is in agreement with the increase in escape fraction seen in CTAC (40%) and CTAB(36%).[85] The aggregation band at 540 nm is not strongly affected by the magnetic field until it reaches 100 mT, at which point aggregation effects are seen across the spectrum. It is likely that the rate of nanoparticle formation reached at this field strength is so great that different modes of aggregation occur; possibly a threshold concentration of nanoparticles is reached, beyond which the surfactant can no longer adequately stabilise the particles. As mentioned earlier, the concentration of CTAN is one quarter of that of SDS; quite likely this concentration is inadequate to stabilise the population of nanoparticles present after irradiation at 100 mT. It is possible that under these conditions, the nanoparticle aggregates themselves

begin to aggregate, forming clusters similar to those seen in the TEM images, which were taken after all the surfactant has been washed off the particles.

1.3.3.2. Effect of Methanol on Surfactant-Stabilised Nanoparticles

Methanol is known to break up SDS micelles.[100] When methanol is added to a solution of nanoparticles prepared from the SDS/BP system with 1,4-CHD, aggregation is immediate. It seems like that the SDS molecules are adsorbed onto the nanoparticle with the hydrophobic tail adjacent to the surface and the hydrophilic head in contact with the solvent, forming a charged layer around the nanoparticle. When this structure is broken up by methanol, the charged layers surrounding and isolating it are lost and the nanoparticles aggregate.

1.3.3.3. Photogeneration of Silver Nanoparticles from Irgacure-2959 in the Absence of Micelles

Since Irgacure-2959 is water-soluble and does not require a hydrogen-donor, micelles are not required to solubilise any of the components of the system. When photolysis is carried out without SDS micelles, the aggregate band is greatly favoured over the discrete particle peak to approximately the same extent that the discrete is favoured over the aggregated when micelles are present (Figure 1.42). This strongly suggests that the anionic micelles maintain the separation of the individual particles, most likely by the hydrophobic tail adsorbing on the surface of the particle, with the

hydrophilic head in contact with the aqueous solution, as described in the previous section. The resulting charged double layer of anionic head and cationic counter layer sets up a coulombic barrier to aggregation.[88]

With no surfactants present, the ketyl radicals are not born in micelles and therefore do not have to escape from confinement. However, the lack of micelles means that there is no layer of silver cations in close proximity to the newly formed ketyl radical.

While SDS plays a distinct role in stabilizing spherical nanoparticles, it is not as efficient a stabiliser as 1,4-CHD. Due to solubility issues, it was not possible to perform photolysis experiments with 1,4-CHD in the absence of SDS micelles, as most of the CHD resides in the micelle. This will be demonstrated in the next section.

1.3.4. Side Reactions During Nanoparticle Formation

1.3.4.1. The Effect of Silver Ion Concentration on Nanoparticle Formation

Reducing the concentration of silver ions from 10 mM to 5 mM in the presence of CHD has the effect of increasing the production of nanoparticles, as indicated by plasmon band formation. This seems counterintuitive, but can be explained by the fact that silver quenches the excited triplet state of benzophenone as shown in the previous section, decreasing the generation of ketyl radicals. Below 5 mM, production also

decreases as quenching effects cease to be dominant and nanoparticle generation is proportional to $[Ag^+]$. It is worth noting that nanoparticle production peaks when the concentrations of silver(I) and benzophenone are equal. Above 10 mM, the plasmon band absorption decreases linearly as the concentration of silver increases, reflecting the increasing quenching of the triplet by Ag^+. The λ_{max} of the plasmon absorption, however, increases as the square of the concentration of silver increases and does not display a local maximum at 5 mM as the absorbance did, suggesting that the phenomenon giving rise to this effect is not affected by the quenching of the benzophenone triplet. This is an empirical observation and not predicted by theory. Increasing the concentration of silver, therefore, results in larger particles. This is the reverse of the trend seen with 1,4-CHD, where an increase in alkene led to smaller particles. The explanation for this is the same: as $[Ag^+]$ increases relative to [1,4-CHD], the amount of alkene available for capping per unit surface area decreases. At first glance, it seems that these effects should not be noticeable, as there is a four-fold excess of diene compared to silver, and most of the silver atoms are buried in the centre of the nanoparticles. Only a tiny fraction of the available 1,4-CHD is needed to stabilise the particles in conjunction with the surfactant molecules. However, most of the diene resides in the micelles and not in solution where the nanoparticle generation occurs; approximately $1/6^{th}$ of silver ions in solution are complexed with 1,4-CHD, according to Equation 1.2 (Table 1.2). As it is in equilibrium, 1,4-CHD can exit the micelle as the molecules in solution adsorb onto the nanoparticle surfaces, but this likely occurs much slower than particle growth. As a result, particle growth is arrested later, resulting in larger particles. The increase seen in peak width can also be explained by an increase in

aggregation resulting from a lower stabiliser/silver ratio. It has been shown that the presence of 1,4-CHD can break up existing aggregates (Figure 1.15), but this process takes time, and the spectra in Figure 1.11 were recorded immediately after irradiation.

Table 1.2 Effects of [Ag^+] on the plasmon absorbance and formation of silver-olefin complex

[Ag^+] (mM)	1,4-CHD:Ag^+	[Ag1,4-CHD^+] [1] (mM)	λ_{max} (nm)	Peak ΔOD	Peak width (nm)
3	13.3	0.59	410	1.5	85
5	8	0.98	412	1.6	96
10	4	1.96	414	1.5	107
15	2.67	2.94	417	1.3	117
20	2	3.92	425	1.1	155
30	1.33	5.88	444	0.68	Off scale

[1]-determined from Equation 1.2

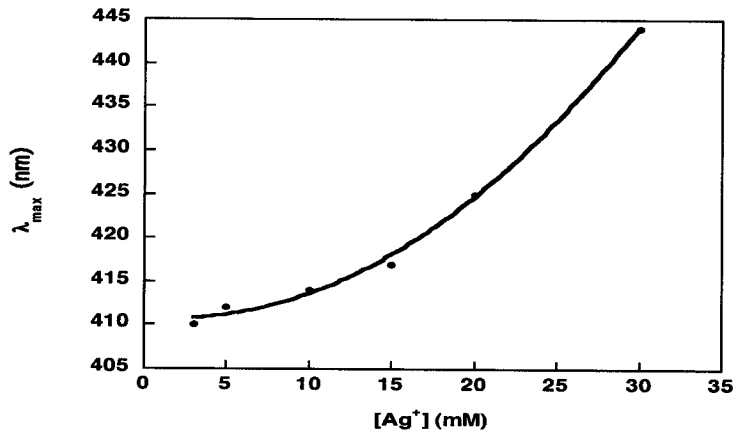

Figure 1.55: Plot of λ_{max} of the plasmon band of silver nanoparticles as a function of $[Ag^+]$ in solutions of 0.1 M SDS, 0.005 M BP and 0.04 M 1,4-CHD following vortex purging and 30 seconds irradiation with an Oriel Xenon lamp and 320 nm cutoff filter. All points have had the pre-irradiation absorbance subtracted.

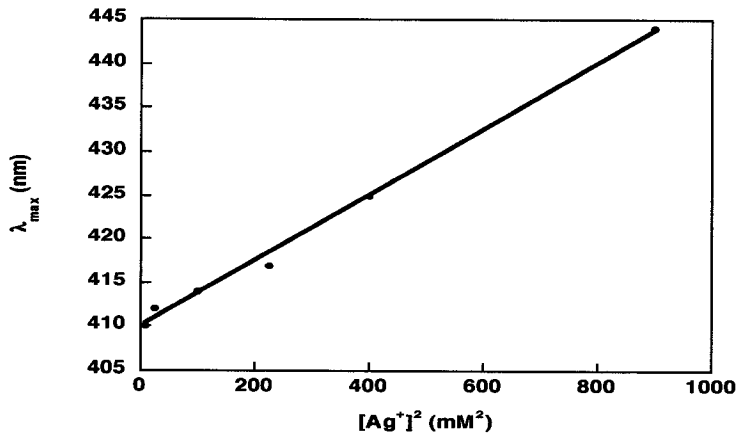

Figure 1.56: Plot of λ_{max} of the plasmon band of silver nanoparticles as a function of the square of $[Ag^+]$ in solutions of 0.1 M SDS, 0.005 M BP and 0.04 M 1,4-CHD following vortex purging and 30 seconds irradiation with an Oriel Xenon lamp and 320 nm cutoff filter. All points have had the pre-irradiation absorbance subtracted.

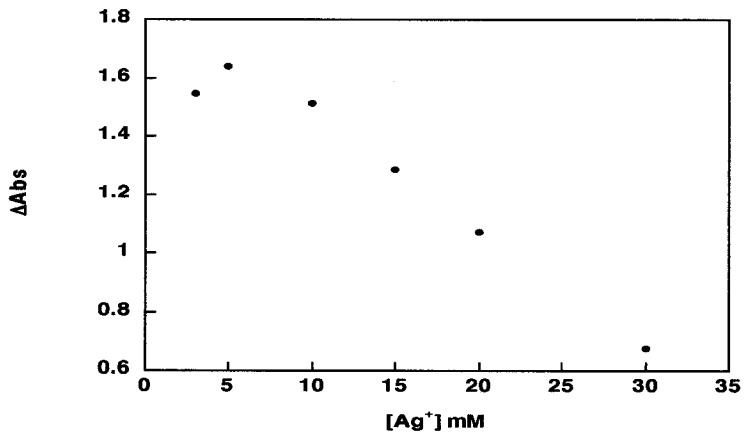

Figure 1.57: Plot of intensity of the absorbance of the plasmon band of silver nanoparticles as a function of [Ag^+] in solutions of 0.1 M sodium dodecyl sulphate, 0.005 M benzophenone and 0.04 M 1,4-cyclohexadiene, following vortex purging and 30 seconds irradiation with an Oriel Xenon lamp and 320 nm cutoff filter. All points have had the pre-irradiation absorbance subtracted.

There are striking differences, however, in the shapes of the plasmon bands between the experiments in which [1,4-CHD] was varied and in which [Ag^+] was varied. When the concentration of silver was kept constant at 10 mM and that of 1,4-CHD was adjusted to 20 mM, the mole ratio of silver to alkene was 0.5. The same ratio was achieved when [1,4-CHD] was kept constant at 40 mM and a silver concentration of 20 mM. A comparison of these two spectra (Figure 1.58) reveals that the solution containing 20 mM Ag^+ gives rise to a broader, less intense plasmon band despite the higher concentration of 1,4-CHD compared to the solution containing 10 mM of silver. Clearly, large amounts of silver are detrimental to the formation of discrete silver nanoparticles.

As the concentration of silver increases, the ratio of stabiliser (whether surfactant or 1,4-CHD) decreases. As a result, less stabiliser is adsorbed per unit surface area of particle, leading to aggregation and the observed broader plasmon bands. This phenomenon has already been discussed in more detail.

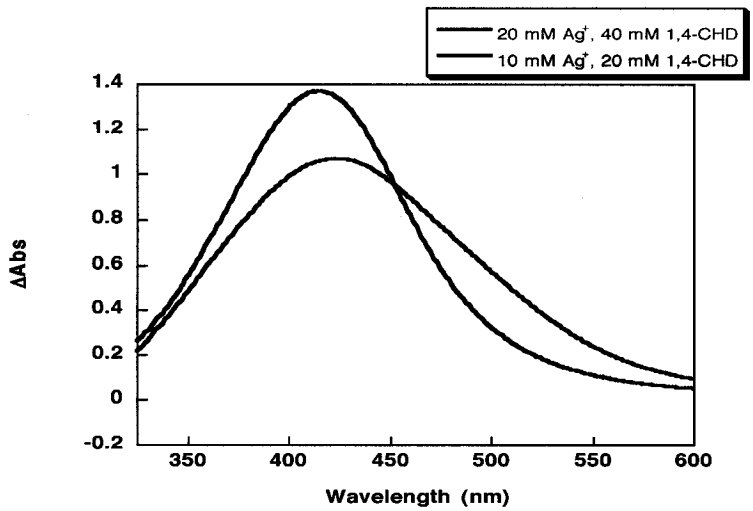

Figure 1.58: Comparison of spectra of silver nanoparticles obtained from solutions of 0.1 M SDS, 0.005 M BP and varying concentrations of $AgNO_3$ and 1,4-CHD following vortex purging and 30 seconds irradiation with an Oriel Xenon lamp and 320 nm cutoff filter. All spectra have had the pre-irradiation absorbance subtracted.

1.3.4.2. Effects of Oxygen During Photogeneration of Nanoparticles

Samples must be flushed with nitrogen prior to irradiation in order to remove all traces of oxygen, which will otherwise interfere with the reaction. Triplet benzophenone

is a singlet oxygen sensitiser, with approximately 30% of BP triplets yielding $^1O_2$.[101] This singlet oxygen can then react with 1,4-CHD through the ene reaction to produce peroxides;[102] the latter has a trivial effect on nanoparticle formation due to the relative concentrations of 1,4-CHD (40 mM) and oxygen (0.286 mM at 20 C and standard atmospheric pressure).[103] The primary source of disruption is the deactivation of benzophenone triplets by molecular oxygen. Figure 1.44 shows the effect of dissolved oxygen on the photogeneration of nanoparticles. Over equal irradiation times, the process is approximately 40% as efficient as it is in the absence of oxygen. In addition, the spectrum shows evidence of considerable aggregation. As the sample was stored in a glovebox in an unsealed cuvette, this is most likely due to aggregation caused by the volatile 1,4-CHD escaping from the solution. An unexpected observation is the shift of the peak to shorter wavelengths with increased irradiation time. It is likely the particles become larger with more irradiation, and hence more stable, and thus disaggregate as a result.

1.3.4.3. Oxygen and Irgacure

The Irgacure-derived ketyl-benzoyl triplet radical pair is quenched by oxygen. After irradiation the absorbance of an unpurged sample is markedly less than that of a purged sample. The shape of the curve, however, is not substantially different, indicating that the quenching by oxygen does not affect the mechanism of nanoparticle formation or the stability of the particles.

1.3.4.4. Studies of the Effects of Exposure to Air on the Generation and Stability of Silver Nanoparticles

In addition to interfering with the production of nanoparticles through oxygen quenching of the benzophenone triplet, air also promotes aggregation of the nanoparticles after photolysis is complete. In addition, samples exposed to nitrogen aggregated at a slower rate. The aggregation noted in N_2 was caused by the loss of the volatile 1,4-CHD. A strong 1,4-CHD odour was noted immediately after the UV cells were unsealed, but it had vanished by the next day following repeated transfers of the solution between the cuvettes and plastic centrifuge tubes. Solutions which were not disturbed, and which were stored in cuvettes with very narrow necks that minimised the loss of 1,4-CHD, displayed minimal aggregation. In addition, the particles continued to grow through Ostwald ripening[51], as evidenced by the increase in the absorbance of the plasmon resonance band. The more rapid aggregation in air was possibly aided by oxidation of the surface of the nanoparticles. Oxygen in the air is known to oxidise nanoparticles,[96] but the resulting Ag_2O particles do not display a plasmon band. This is because the plasmon absorbance is a surface effect, oxidising the surface will destroy the oscillation of the electrons that gives rise to this absorbance. However, silver is a known oxidation catalyst for alkenes,[104] so it is likely that the vast surface area of the nanoparticles is oxidising the 1,4-CHD, which then effectively destroys the stabilizing coating and promotes aggregation.

1.4. Conclusion

Applied magnetic fields have been conclusively demonstrated to enhance the rate of formation of silver nanoparticles in the system under investigation. A linear relationship between plasmon band intensity and magnetic field strength was observed up to 750 mT. In addition, the presence of 1,4-cyclohexadiene dramatically increased not only the rate of photogeneration of nanoparticles by contribution to the formation of benzophenone ketyl radicals through hydrogen donation, but also to the stability of the particle by adsorbing on the surface. Magnetic field effects were also seen when benzhydrol was used as a hydrogen donor, and in cationic cetyltrimethylammonium nitrate micelles, and barely observed with Irgacure-2959 as a source of ketyl radicals. An increase in the concentration of Ag^+ actually caused a decrease in the production of nanoparticles due to the quenching of the triplet state of benzophenone by silver. The particles obtained from the SDS/BP/CHD system were stable for long periods of time, on the order of weeks, as long as the cuvettes in which they were irradiated remained sealed; otherwise, exposure to oxygen and loss of 1,4-CHD through evaporation resulted in rapid aggregation and oxidation.

1.5. Experimental

1.5.1. Materials

All chemicals were acquired from Aldrich unless otherwise indicated. Silver nitrate and silver perchlorate from Alfa Aesar were stored in a desiccator when not in use. 1,3-Cyclohexadiene was distilled and stored under nitrogen. Benzhydrol was purified by hot gravity filtration. 1,4-Cyclohexadiene, benzophenone from BHD, sodium dodecyl sulphate from Fisher Scientific, and cetyltrimethylammonium bromide were used without further purification.

1.5.2. General Techniques

1.5.2.1. Photolysis

Samples were prepared first making up a 100 mM solution of SDS in a 50 mL volumetric flask and adding 0.250 mL of 1M benzophenone in methanol to produce a final BP concentration of 5 mM. The solution was made up to volume and 3 mL was transferred to 10 x 10 mm UV-grade fused silica Luzchem cuvettes, to which was added 150 μL of 200 mM $AgNO_3$ stock solution shortly before the experiment to produce $[Ag^+]$ of 10 mM. The cuvettes were then sealed with toluene-washed 0.7 cm outer diameter septa and wrapped with Parafilm. Samples were deoxygenated with an 8-minute headspace purge followed by an 8-minute vortex purge using a Maximix vortex mixer in order to minimise foaming. 12 μL of 1,4-cyclohexadiene was added to the

cuvettes subsequent to purging by injection through the septa. Samples were then vortex mixed for 5 s to mix the 1,4-CHD and vortex purged again for 10 s to remove traces of oxygen added during injection, and more Parafilm was used to complete seal the septa. After purging, spectra were recorded on a Cary 50 Bio spectrophotometer from Varian. Irradiations were carried out using a 150 W Oriel CW Xenon lamp. The irradiation wavelength was selected with a 320 nm cutoff filter. Magnetic fields were applied with a home built electromagnet capable of DC fields up to 1200 G (120 mT). The sample was placed in a 10 x 10 mm brass sample holder located between the poles of a 15 cm diameter electromagnet. The sample was located 25 cm from the aperture of the lamp. UV/Visible spectra were acquired immediately after irradiation, and the pre-irradiation spectra were then subtracted to determine the net increase in absorption. Magnetic fields were determined with an Alphalab gaussmeter.

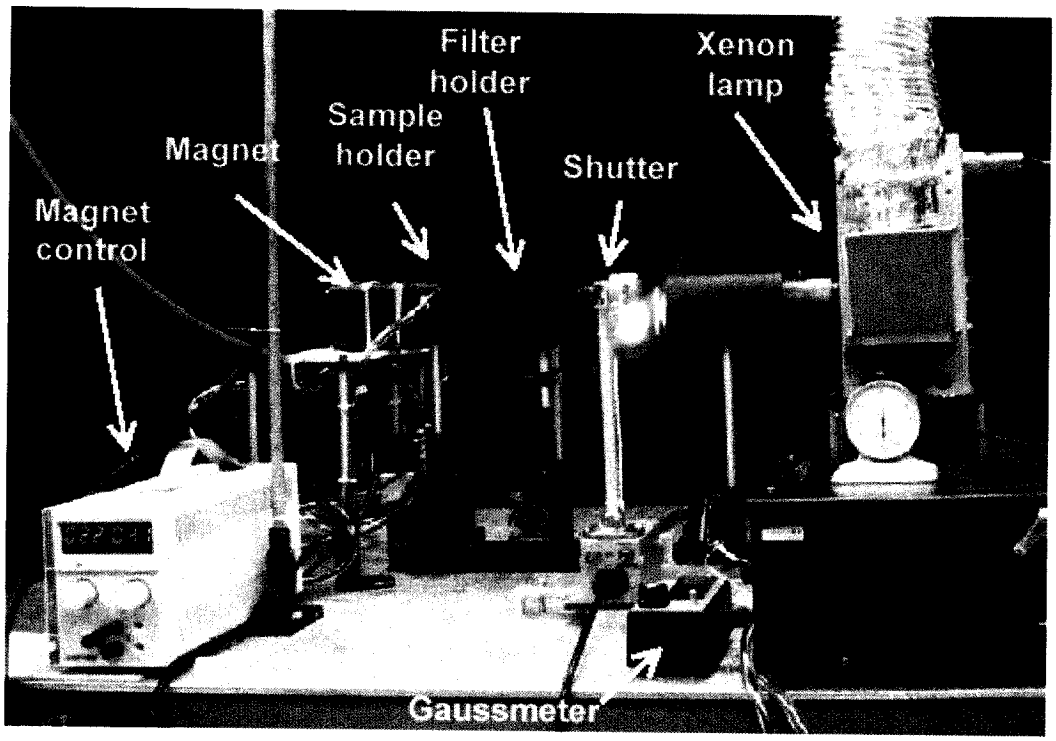

Figure 1.59: Photograph of photolysis experimental setup.

1.5.2.2. Infrared Spectroscopy

IR spectra were acquired on ThemoNicolet Nexus 670 FT-IR spectrometer connected to a Parker Filtration purge gas generator. Samples were prepared by dissolving $AgNO_3$ and 1,4-CHD in ACN, pipetting the solution over NaCl plates and allowing the solvent to evaporate.

1.5.2.3. Laser Flash Photolysis

Nanosecond laser flash photolysis measurements were acquired using the third harmonic from a Continuum Surelight Nd-YAG laser (355 nm, ~6 ns pulse width, ~12

mJ/pulse). Signals were acquired using a Digikrom monochromator and a Hamamatsu 928 photomultiplier and a Tektronix oscilloscope and output to a desktop PC running mLFP software from LuzChem. All samples were purged under nitrogen as described earlier, and all experiments were carried out at room temperature. During quenching experiments, samples were shaken periodically to reduce localized buildup of reduced silver that could form nanoparticles.

1.5.2.4. Transmission Electron Microscopy

TEM images were acquired on a Philips CM20 STEM equipped with a Gatan UltraScan 1000 CCD camera and an energy dispersive x-ray spectrophotometer (EDS) at the National Research Council of Canada's Institute for Chemical Process and Environmental Technology (ICPET). Samples were prepared within three hours of nanoparticle synthesis by transferring 10 μL of solution to a 300 mesh copper TEM grid with carbon coating. The grids were subsequently washed with methanol to remove surfactants and unreacted silver salt in order to improve picture quality. The TEM was operated at 200 kV.

1.5.3. Synthesis

1.5.3.1. Cetyltrimethylammonium nitrate

CTAN was prepared from cetyltrimethylammonium chloride and bromide (CTAC and CTAB) by precipitation with $AgNO_3$. To an aqueous solution of surfactant, stoichiometric amounts of methanolic $AgNO_3$ were added until precipitation of silver halide was observed to cease. The resulting solution was filtered and the CTAN was collected by rotary evaporation and dried over a vacuum pump. The CTAN crystals were then redissolved in sparing amounts of ethanol and precipitated twice with diethyl ether to remove impurities – additions of $AgNO_3$ and NaCl to subsamples of the product did not result in precipitates, indicating no contamination by X^- and Ag^+, respectively. Typical yields were ~25%.

1.6. References

1. Roco, M.C., *International strategy for Nanotechnology Research.* J. Nanop. Res., 2001. **3**(5-6): p. 353-60.
2. Kopf, H., Joshi, R.K., Soliva, M. and Speiser, P., *Study on micelle polymerisation in the presence of low-molecular-weight drugs. 1. Production and isolation of nanoparticles, residual monomer determination, physical-chemical data.* Pharmazeutische Industrie, 1976. **38**(3): p. 281-4.
3. Daniel, M.-C. and Astruc, D., *Gold Nanoparticles: Assembly, Supramolecular Chemistry, Quantum-Size-Related Properties, and Applications towards Biology, Catalysis and Nanotechnology.* Chem. Rev., 2004. **104**: p. 293-346.
4. Thomas, T., Thomas, K., Sadrieh, N., Savage, N., Adair, P. and Bronaugh, R., *Research Strategies for Safety Evaluation of Nanomaterials.* Toxicological Studies, 2006. **91**(1): p. 14-19.
5. Lu, Y., Fan, H., Stump, A., Ward, T., Rieker, T. and Brinker, C.J., *Aerosol-assisted Self-assembly of Mesostructured Spherical Nanoparticles.* Nature, 1999. **398**(6724): p. 223.
6. Petroski, J.M., Wang, Z.L., Green, T.C. and El-Sayed, M., *Kinetically Controlled Growth and Shape Formation Mechanism of Platinum Nanoparticles.* J. Phys. Chem. B, 1998. **102**: p. 3316-20.
7. Chen, H., Gao, Y., Zhang, H., Liu, L., Yu, H., Tian, H., Xie, S. and Li, J., *Transmission-Electron-Microscopy Study on Fivefold Twinned Silver Nanorods.* J. Phys. Chem. B, 2004. **108**: p. 12038-43.
8. Zhang, F., Chan, S., Spanier, J.E., Apak, E., Jin, Q., Robinson, R.D. and Herman, I.P.
9. Zhao, N. and Qi, L., *Low-Temperature Synthesis of Star-Shaped PbS Nanocrystals in Aqueous Solutions of Mixed Cationic/Anionic Surfactants.* Adv. Mater, 2006. **18**(3): p. 359-62.
10. Deotare, P.B. and Kameoka, J., *Fabrication of Silica Nanocomposite-cups Using Electrospraying.* Nanotechnology, 2006. **17**: p. 1380-3.
11. Hayashida, T., Pan, L. and Nakayama, Y., *Mechanical and Electrical Properties of Carbon Tubule Nanocoils.* Physica B, 2002. **323**: p. 352-3.
12. Li, X.L., Liu, J.F. and Li, Y.D., *Low-temperature Conversion Synthesis of M(OH)2 (M-Ni, Co, Fe) Nanoflakes and Nanorods.* Mater. Chem. Phys., 2003. **80**(1): p. 222-7.
13. Shirai, Y., Osgood, A.J., Zhao, Y., Kelly, K.F. and Tour, J.M., *Directional Control in Thermally Driven Single-Molecule Nanocars.* Nano Lett., 2005. **5**: p. 2330-4.
14. Morin, J.-F., Shirai, Y. and Tour, J.M., *En Route to a Motorised Nanocar.* Org. Lett., 2006. **8**(8): p. 1713-6.
15. Singh, P.K., *Dispersion of Nanoparticulate Suspensions Using Self-Assembled Surfactant Aggregates*, in *Department of Chemistry.* 2002, University of Florida: Gainesville. p. 181.
16. *Modern Developments in Electron Microscopy*, ed. B.M. Siegel. 1964, New York: Academic Press.

17. Yu, A.C.C., Mizuno, M., Sasaki, Y., Inoue, M., Kondo, H., Ohta, I., Djayaptawira, D. and Takahashi, M., *Fabrication of Monodispersive FePt Nanoparticle Films Stabilised On Rigid Substrates*. Appl. Phys. Lett, 2003. **82**(24): p. 4352-4.
18. Cheung, C.L., Hafner, J.H. and Lieber, C.M., *Carbon Nanotube Atomic Force Microscopy Tips: Direct Growth by Chemical Vapour Deposition and Application to High-resolution Imaging*. PNAS, 2000. **97**(8): p. 3809-13.
19. Zhang, H. and Yang, B., *X-ray Photoelectron Spectroscopy Studies of the Surface of Highly Luminescent CdTe Nanoparticles in Multilayer Films*. Thin Solid Films, 2002. **418**(2): p. 169-74.
20. El Sayed, M.A., *Small Is Different: Shape-, Size- and Composition-Dependent Properties of Some Colloidal Semiconductor Nanocrystals*. Acc. Chem. Res., 2004. **37**(326-333).
21. Zhu, H.-T., Zhang, C.-Y. and Yin, Y.-S., *Rapid synthesis of copper nanoparticles by sodium hypophosphite reduction in etheylene glycol under microwave irradiation*. J. Cryst. Growth, 2004. **270**(3-4): p. 722-8.
22. Zhang, Y., Chen, F., Zhuang, J., Tang, Y. and al, e., *Synthesis of silver nanoparticles via electrochemical reduction on compact zeolite film modified electrodes*. Chem. Comm., 2002: p. 2814-2815.
23. Wagner, J. and Kohler, J.M., *Continuous synthesis of gold nanoparticles in a microreactor*. Nanolatters, 2005. **5**(4): p. 685-91.
24. Rosemary, M.J. and T., P., *Solvothermal synthesis of silver nanoparticles from thiolates*. Journal of colloid and interface science, 2003. **268**(1): p. 81-4.
25. Qi, L., Ma, J. and Shen, J., *Synthesis of copper nanoparticles in nonionic water-in-oil microemulsions*. J. Coll. Interf. Sci., 1997. **168**(2): p. 498-500.
26. Kim, K.-S., Choi, S., Cha, J.-H., Yeon, S.-H. and Lee, H., *Facile one-pot synthesis of gold nanoparticles using alcohol ionic liquids*. J. Mater. Chem., 2006. **16**(14): p. 1315-7.
27. de Cuendias, A., Backov, R., Cloutet, E. and Cramail, H., *Synthesis of gold nanoparticles coated onto polyurethane microspheres*. J. Mater. Chem., 2005. **15**(39): p. 4196-9.
28. Li, Y., Wu, Y. and Ong, B.S., *Facile Synthesis of silver nanoparticles useful for fabrication of high-conductivity elements for printed electronics*. J. Am. Chem. Soc., 2005. **127**(10): p. 3266-7.
29. Song, X., Sun, S., Zhang, W. and Yin, Z., *A method for the synthesis of spherical copper nanoparticles in the organic phase*. J. Coll. Interf. Sci., 2004. **273**(2): p. 463-9.
30. Verelst, M., Ely, T.O., Amiens, C., Snoeck, E., Lecante, P., Mosset, A., Respaud, M., Broto, J.M. and Chaudret, B., *Synthesis and Characterisation of CoO, Co3O4 and Mixed Co/CoO Nanoparticles*. Chem. Mater., 1999. **11**(10): p. 2702-8.
31. Xing, Y., Kole, T.P. and Katz, J.L., *Shape-controlled synthesis of iron oxide nanoparticles*. J. Mater. Sci. Lett., 2003. **22**(11): p. 787-90.
32. Yang, H., Hu, Y., Zhang, X. and Qiu, G., *Mechanochemical synthesis of cobalt oxide nanoparticles*. Mater. Lett., 2003. **58**(3-4): p. 387-9.

33. Lim, S.K., Chung, K.J., Kim, Y.-H., Kim, C.K. and Yoon, C.S., *Synthesis of iron oxide nanoparticles in a polyimide matrix.* J. Coll. Interf. Sci., 2004. **60**(1-3): p. 151-8.
34. Park, S.M., Ki, W., Yu, J. and Du, H., *Sol-gel synthesis of highly dispersed cobalt nanoparticles on silica thin films.* J. Mater. Res., 2005. **20**(11): p. 3094-3101.
35. Wang, Y., Zhu, J., Yang, X., Lu, L. and Wang, X., *Preparation of NiO nanoparticles and their catalytic activity in the thermal decomposition of ammonium perchlorate.* Thermochim. Acta, 2005. **437**(1-2): p. 106-9.
36. Chaianansutcharit, S., Mekasuwandumrong, O. and Praserthdam, P., *Effect of Organic Solvents on Iron Oxide Nanoparticles.* Crystal Growth & Design, 2006. **6**(1): p. 40-5.
37. Dharmaraj, N., Prabu, P., Nagarajan, S., Kim, C.H., Park, J.H. and Kim, H.Y., *Synthesis of nickel oxide nanoparticles using nickel acetate and poly (vinyl acetate) precursor.* Mater. Sci & Eng B, 2006. **128**(1-3): p. 111-4.
38. Ghosh, M., Biswas, K., Sundaresan, A. and Rao, C.N.R., *MnO and NiO nanoparticles: synthesis and magnetic properties.* J. Mater. Chem., 2006. **16**(1): p. 106-11.
39. Hirasawa, M., Ichikawa, N., Egashira, Y., Honma, I. and Komiyama, H., *Synthesis of GaAs nanoparticles by digital radio frequency sputtering.* Appl. Phys. Lett., 1995. **67**(23): p. 3483-5.
40. Trindade, T. and O'Brien, P., *Synthesis of CdS and CdSe nanoparticles by thermolysis of diethyldithio- or diethyldiseleno-carbamates of cadmium.* J. Mater. Chem., 1996. **6**(3): p. 343-7.
41. Mastai, Y., Polsky, R., Koltypin, Y., Gedanken, A. and Hodes, G., *Pulsed Sonoelectrochemical Synthesis of Cadmium Selenide Nanoparticles.* J. Am. Chem. Soc., 1999. **121**(43): p. 10047-52.
42. Malik, M.A., O'Brien, P., Norager, S. and Smith, J., *Gallium arsenide nanoparticles: synthesis and characterisation.* J. Mater. Chem., 2003. **13**(10): p. 2591-5.
43. Malik, M.A.A., M.; O'Brien P.; Bangert, U.; Hamilton, B., *Single Molecular precusor for synthesis of GaAs nanoparticles.* Mater. Sci. & Tech., 2004. **20**(8): p. 959-63.
44. Yordanov, G.G., Dushkin, C.D., Gicheva, G.D., Bochev, B.H. and Adachi, E., *Synthesis of high-quality semiconductor nanoparticles in a composite hot-matrix.* Colloid and Polymer Science, 2005. **284**(2): p. 229-32.
45. Haes, A.J. and Van Duyne, R.P., *A Nanoscale Optical Biosensor: Sensitivity and Selectivity of an Approach Based on the Localised Surface Plasmon Resonance Spectroscopy of Triangular Silver Nanoparticles.* J. Am. Chem. Soc., 2002. **124**: p. 10596-604.
46. Fendler, J.H., *Chemical Self-assembly for Electronic Applications.* Chem . Mater., 2001. **13**: p. 3196-210.
47. Spiro, M. and De Jesus, D.M., *Nanoparticle Catlysis in Microemulsions: Oxidation of N,N-Dimethyl-p-phenylenediamine by Cobalt(III) Pentaamine Chloride Catalysed by Colloidal Palladium in Water/AOT?n-Heptane Microemulsions.* Langmuir, 2000. **16**(6): p. 2464-8.

48. Johnson, B.F.G., *Nanoparticles in Catalysis.* Topic in Catalysis, 2003. **24**(1-4): p. 147-59.
49. Toshima, N., *Metal nanoparticles for catalysis.* Nanoscale Mater., 2003: p. 79-96.
50. Troiani, H.E., Camacho-Bragado, A., Armendariz, V., Gardea Torresday, J.L. and Jose Yacaman, M., *Synthesis of Carbon Onions by Gold Nanoparticles and Electron Irradiation.* Chem. Mater., 2003. **15**(5): p. 1029-31.
51. Wang, Q. and Ostafin, A.E., *Metal nanoparticles in catalysis.* Encycl. of Nanosci. & Nanotech., 2004. **5**: p. 475-503.
52. Zhang, Z.-F., Cui, H., Lai, C.-Z. and Liu, L.-J., *Gold nanoparticle-catalysed luminol chemiluminescence and its analytical applications.* Anal. Chem., 2005. **77**(10): p. 3324-9.
53. Dabbousi, B.O., Rodrieguez-Veijo, J., Mikulec, F.V., Heine, J.R., Mattoussi, H., Ober, R., Jensen, K.F. and Bawendi, M.G., *(CdSe) ZnS Core-Shell Quantum Dots: Synthesis and Characterisation of a Size Series of Highly Luminescent Nanocrystallites.* J. Phys. Chem. B, 1997. **101**(46): p. 9463-75.
54. Giannelis, E.P., *Polymer-layered Silicate Nanocomposites.* Adv. Mater, 1996. **8**(1): p. 29-35.
55. Yeo, S.Y., Lee, H.J. and Jeong, S.H., *Preparation of Nanocomposite Fibers for Permanent Antibacterial Effect.* J. Mater. Sci., 2003. **38**(10): p. 2143-7.
56. Hong, R.Y., Qian, J.Z. and Cao, J.X., *Synthesis and characterisation of PMMA grafted ZnO nanoparticles.* Powder Technology, 2006. **163**(3): p. 160-8.
57. Hu, Z., Oskam, G. and Searson, P.C., *Influence of solvent on the growth of ZnO nanoparticles.* J. Coll. Interf. Sci., 2003. **263**(2): p. 454-60.
58. Husein, M., Rodil, E. and Vera, J.H., *Formation of silver bromide precipitate of nanoparticles in a single microemulsion utilising the surfactant counterion.* J. Coll. Interf. Sci., 2004. **273**(2): p. 426-34.
59. Huang, X. and Chen, Z., *A Study of nanocrystalline NiFe2O4 in a silica matrix.* Mater. Res. Bull., 2005. **40**(1): p. 105-113.
60. Ellsworth, M.W. and Gin, D.L., *Recent advances in the design and synthesis of polymer-inorganic nanocomposites.* Polymer News, 1999. **24**(10): p. 331-41.
61. Pillai, S.C., Kelly, J.M., McCormack, D.E. and Ramesh, R., *Self-assembled arrays of ZnO nanoparticles and their application as varistor materials.* J. Mater. Chem., 2004. **14**(10): p. 1572-8.
62. Yoshiro, Y., Tomoo, S., Shigeru, K. and Ken-ichi, K., *Photochemical Formation of Colloidal Silver: Peptising Action of Acetone Ketyl Radical.* J. Chem. Soc. Faraday Trans., 1991. **87**(12): p. 1905-1910.
63. Gaddy, G.A., McLain, J.L., Steigerwalt, E.S., Broughten, R., B.L., S. and Mills, G., *Photogeneration of Silver Particles in PVA Fibres and Films.* J. Cluster Sci., 2001. **12**: p. 457-471.
64. Gaddy, G.A., McLain, J.L., Korchev, A.S., Slaten, B.L. and Mills, G., *Kinetics of Silver Particle Photogeneration in Crosslinked PVA/PAA Films.* J. Phys. Chem. B, 2004. **108**: p. 14858-14865.
65. Gaddy, G.A., Korchev, J.L., McLain, J.L., Slaten, B.L., Steigerwalt, E.S. and Mills, G., *Light-Induced Formation of Silver Particles and Clusters in Crosslinked PVA/PAA Films.* J. Phys. Chem. B, 2004. **108**: p. 14850-14857.

66. Callegari, A., Tonto, D. and Chergui, M., *Photochemically Grown Silver Nanoparticles with Wavelength-Controlled Size and Shape*. Nanoletters, 2003. **3**(11): p. 1565-1568.
67. Korchev, A.S., Bozack, M.J., Slaten, B.L. and Mills, G., *Polymer-Initiated Photogeneration of Silver Nanoparticles in SPEEK/PVA Films: Direct Metal Photopatterning*. J. Am. Chem. Soc., 2004. **126**: p. 10-11.
68. Eustis, S., Krylova, G., Eremenko, A., Smirnova, N., Schill, A.W. and El-Sayed, M., *Growth and fragmentation of silver nanoparticles in their synthesis with a fs laser and CW light by photo-sensitisation with benzophenone*. Photochem. Photobiol. Sci., 2005. **4**: p. 154-159.
69. Sudeep, P.K. and Kamat, P.V., *Photosensitised Growth of Silver Nanoparticles under Visible Light Irradiation: A Mechanistic Investigation*. Chem. Mater., 2005. **17**: p. 5404-5410.
70. Burda, C., Chen, X., Narayanan, R. and El-Sayed, M., *Chemistry and Properties of Nanocrystals of Different Shapes*. Chemical Reviews, 2005. **105**: p. 1025-1102.
71. Voorhees, P.W., *The Theory of Ostwald Ripening*. J. Stat. Phys., 1984. **38**(1/2): p. 231-51.
72. Haik, Y., Chatterjee, J. and Chen, C.J., *Synthesis and Stabilisation of Fe-Nd-B Nanoparticles for Biomedical Applications*. J. Nanop. Res., 2005. **7**(6): p. 675-79.
73. Sau, T.K., Pal, A., Jana, N.R., Wang, Z.L. and Pal, T., *Size controlled synthesis of gold nanoparticles using photochemically prepared seed particles*. J. Nanop. Res., 2001. **3**(257-61).
74. Abid, J.P., Wark, A.W., Brevet, P.F. and Girault, H.H., *Preparation of silver nanoparticles in solution from a silver salt by laser irradiation*. Chem Comm., 2002: p. 792-793.
75. Micic, O.I., Curtis, C.J., Jones, K.M., Sprague, J.R. and Nozik, A.J., *Synthesis and Characterisation of InP Quantum Dots*. J. Phys. Chem., 1994. **98**: p. 4966-9.
76. Zhong, Z., Male, K.B. and Luong, J.H.T., *More Recent Progress in the Preparation of Au Nanostructures, Properties and Applications*. Anal. Lett., 2003. **36**(15): p. 3097-118.
77. Peng, Z.A. and Peng, Z., J. Am. Chem. Soc., 2002. **124**: p. 3343.
78. Purcell, E.M., *Electricity and Magnetism*. Berkeley Physics Course. Vol. 2. 1965, Berkeley: McGraw-Hill.
79. Berry, M.V. and Geim, A.K., *Of Flying Frogs and Levitrons*. Eur. J. Phys., 1997. **18**: p. 307-313.
80. Griffiths, D.J., *Introduction to Quantum Mechanics (2nd. Ed.)*. 2004: Prentice Hall.
81. Nawa, M., Baba, R., Nakabayashi, S. and Dushkin, C., Nano Letters, 2003. **3**: p. 293-7.
82. Halteen, J.C., Treichel, D.A., Smith, M.T., Duval, M.L., Jensen, T.R. and van Duyne, R.P., *Nanosphere Lithography: Size-Tunable silver nanoparticle and Surface Cluster Arrays*. J. Phys. Chem. B, 1999. **103**: p. 3854-63.
83. Chou, S.Y., Krauss, P.R., Zhang, W., Guo, L. and Zhuang, L., J. Vac. Sci. Technol. B, 1997. **15**: p. 2897-2904.

84. Chou, S.Y., Proc. IEEE, 1997. **85**: p. 652-71.
85. Scaiano, J.C., Abuin, E.B. and Stewart, L.C., *Photochemistry of Benzophenone in Micelles. Formation and Decay of Radical Pairs.* J. Am. Chem. Soc., 1982. **104**: p. 5673-5679.
86. Murov, S.L.C., *Handbook of Photochemistry.* 2nd ed, ed. G.L. Hug. 1993, New York: Marcel Dekker, Inc.
87. Fendler, J.H., *Membrane Mimetic Chemistry.* 1st ed. 1982, Toronto: John Wiley & Sons.
88. Moskovits, M. and Vlckova, B., *Adsorbate-Induced Silver Nanoparticle Aggregation Kinetics.* J. Phys. Chem. B, 2005. **109**(31): p. 14755-14758.
89. Patterson, M.L. and Weaver, M.J., *Surface-enhanced Raman spectroscopy as a probe of adsorbate-surface bonding: simple alkenes and alkynes adsorbed at gold electrodes.* J. Phys. Chem., 1985. **89**(23): p. 5046-51.
90. Muhs, M.A. and Weiss, F.T., *Determination of Equilibrium Constants of Silver-Olefin Complexes Using Gas Chromatography.* J. Am. Chem. Soc., 1962. **84**: p. 4697-705.
91. Elecgiguerra, J.L., Larios-Lopez, L., Liu, C., Garcia-Gutierrez, D., Camacho-Bragado, A. and Yacaman, M.J., *Corrosion at the Nanoscale: The Case of Silver Nanowires and Nanoparticles.* Chem. Mater., 2005. **17**(24): p. 6042-52.
92. Pouchert, C.J., *The Aldrich Library of Infrared Spectra.* 1975, Milwaukee: Aldrich Chemical Co.
93. Moskovits, M., Rev. Mod. Phys., 1985. **57**: p. 783.
94. Takeda, K., Kajii, Y., Shibuya, K. and Obi, K., *Heats of formation of intermediate radicals in solution.* J. Photochem. Photobiol. A, 1998. **115**(2): p. 109-15.
95. DePierro, M.A., Olson, A.J. and Cuymon, C.A., *Effect of photoinitiator segregation on polymerisation kinetics in lyotropic liquid crystals.* Polymer, 2004. **46**(2): p. 335-345.
96. Egorova, E.M. and Revina, A.A., *Optical Properties and Sizes of Silver Nanoparticles in Micellar Solutions.* Coll. J., 2001. **64**(3): p. 301-311.
97. Lide, D.R., ed. *CRC Handbook of Chemistry and Physics.* 85 ed. 2004, CRC Press: New York.
98. Bunton, C.A. and Cerichelli, G., Int. J. Chem. Kinet., 1980. **11**: p. 519.
99. Chidambaram, N. and Burgess, D.J., *Effect of Cationic Surfactant on Transport of Surface-Active and Non-Surface-Active Model Drugs and Emulsion Stability in Triphasic Systems.* AAPS PharmSci, 2000. **2**(3).
100. Chauhan, M.S., Kumar, G., Kumar, A., Sharma, K. and Chauhan, S., *Conductance and viscosity studies of sodium dodecylsulphate in aqueous solutions of dimethylsulfoxide and methanol.* Coll. Surf. A, 2000. **180**(1-2): p. 111-119.
101. Firey, P.A., Ford, W.E., Sounik, J.R., Kenney, M.E. and Rodgers, M.A.J., J. Am. Chem. Soc., 1988. **110**(23): p. 7626-30.
102. Hoffman, H.M.R., *The Ene Reaction.* Angew. Chem., Int.Ed. Engl., 1969. **8**: p. 556.

103. McDonagh, C., MacCraith, B.D. and McEvoy, A.K., *Tailoring of Sol-Gel Films for Optical Sensing of Oxygen in Gas and Aqueous Phase*. Anal. Chem., 1998. **70**: p. 45-50.
104. Roberts, J.T. and Madix, R.J., *Epoxidation of olefins on silver: conversion of norbornene to norbornene oxide by atomic oxygen on silver (110)*. J. Am. Chem. Soc., 1988. **110**(25): p. 8540-1.

2. Claims to Original Research

1) Demonstrating that Zeeman splitting of the triplet state of benzophenone caused by an externally applied magnetic field increases the rate of photogeneration of silver nanoparticles under mild conditions

2) Demonstrating that adsorbed, uncharged organic species such as dienes and surfactants can stabilise silver nanoparticles and reverse aggregation.

3) Establishing that the photoreduction of silver nanoparticles occurs readily under mild conditions despite the quenching effect of silver on benzophenone triplets and in the presence of oxygen.

4) Demonstrating the first known photogeneration of silver nanoparticles from an Irgacure system lacking a separate hydrogen donor.

Publications resulting from work presented in this thesis

[1] JC Scaiano, C Aliaga, S Maguire, D Wang, "Magnetic Field Control of Photoinduced Silver Nanoparticle Formation," *J. Phys. Chem. B*, **110** (26), 12856 – 12859, **2006.**